ELEMENTAL AND ISOTOPIC CHEMISTRY OF THE UZON CALDERA: THE EVOLUTION OF THERMAL WATERS, GAS, AND MINERAL PRECIPITATION

by

ELIZABETH R. HOLLINGSWORTH

(Under the Direction of Douglas E. Crowe)

ABSTRACT

The Uzon Caldera is an active As-Sb-Au epithermal system of the Kamchatka Peninsula, Far-East Russia. Using $\delta D/\delta^{18}O/\delta^{34}S$ and dissolved ion chemistry, three thermal fluid types were distinguished at the surface as follows: 1) an acid sulfate type 2) an alkali chloride type and 3) a dilute type resulting from the mixing of alkali chloride and cold surface meteoric fluid components. Interpretations made from the presence of these three thermal fluid types were used in conjunction with the $\delta^{34}S$ of the S-bearing alteration minerals found within and around the various water and gas sources to construct a sulfur evolution model for the caldera's hydrothermal system. Model results show the chemical and isotopic processes responsible for the speciation and isotopic signature of the S-bearing phases collected at the surface (both aqueous and mineral) are not only dictated by geology at depth, but are also influenced by microbial processes at the surface.

INDEX WORDS: Uzon Caldera, Hydrothermal System, Isotopes, Sulfur Modeling

ELEMENTAL AND ISOTOPIC CHEMISTRY OF THE UZON CALDERA: THE EVOLUTION OF THERMAL WATERS, GAS, AND MINERAL PRECIPITATION

by

ELIZABETH R. HOLLINGSWORTH

B.S., The University of the South, 2003

A Thesis Submitted to the Graduate Faculty of The University of Georgia in Partial Fulfillment of the Requirements for the Degree

MASTER OF SCIENCE

ATHENS, GEORGIA

2006

ELEMENTAL AND ISOTOPIC CHEMISTRY OF THE UZON CALDERA: THE EVOLUTION OF THERMAL WATERS, GAS, AND MINERAL PRECIPITATION

by

ELIZABETH R. HOLLINGSWORTH

Major Professor:	Doug E. Crowe
Committee:	Paul A. Schroeder
	Christopher S. Romanek

Electronic Version Approved:
Maureen Grasso
Dean of the Graduate School
The University of Georgia
May 2006

ACKNOWLEDGEMENTS

This research was generously supported by the NSF's Kamchatka Microbial Observatory (Grant No. 0238407) with additional funding from the University of Georgia's Department of Geology (Wheeler/Watts Grant). Thanks to Dr. Christopher Romanek (SREL) for his analysis of the $\delta D/\delta^{18}O$ isotope data, Mrs. Julia Cox (UGA) for her patient assistance with the $\delta^{34}S$ isotope analyses, Mr. Morris Jones (SREL) for the IC analysis, the Chemical Analysis Laboratory (UGA) for the ICP-MS analysis, and Dr. Douglas Crowe (UGA) for sediment size fractioning the core samples. Also thanks to Drs. Douglas Crowe and Paul Schroeder (UGA) for the use of their lab facilities. I also appreciate the work put in by Dr. Douglas Crowe, Dr. Christopher Romanek, Ms. Jennifer Kyle, and Ms. Carrie-Ayne Jones in helping to collect many of the samples used to piece together this research.

I would also like to acknowledge all of the Microbial Observatory's Russian colleagues who's participation and dedication to the goal of making science an international collaborative venture, has made this project possible.

TABLE OF CONTENTS

Page

ACKNOWLEDGEMENTS iv

LIST OF TABLES vii

LIST OF FIGURES viii

CHAPTER

1 INTRODUCTION 1

1.1 Regional Geology 1

1.2 Geologic History of Uzon 4

1.3 The Hydrothermal System of Uzon 5

2 METHODS 17

2.1 Field Methods 17

2.2 Lab Methods 17

3 RESULTS 20

3.1 Water Chemical, δD, $\delta^{18}O$, and $\delta^{34}S$ Isotope Geochemistry 20

3.2 Mineral $\delta^{34}S$ Isotope Geochemistry 27

4 DISCUSSION 36

4.1 Water Chemical and δD/$\delta^{18}O$ Isotope Geochemistry 36

4.2 Rock Mineral $\delta^{34}S$ Compositions 43

4.3 Water $\delta^{34}S$ Sulfate Compositions 46

4.4 Core Sample Mineral $\delta^{34}S$ Compositions 60

5 CONCLUSIONS....64

REFERENCES....65

APPENDICES....70

A RESULTS OF EXPERIMENTAL METHOD TESTS....70

B XRD DATA USED TO INTERPRET MINERALOGY OF SAMPLES....72

C DETAILED LOG OF SULFUR ISOTOPE DATA FOR ALL SAMPLES....84

LIST OF TABLES

Page

Table 1: Chemical and stable isotope data for water samples 21

Table 2: Isotope data for fumarole precipitates and vapor alteration minerals.....28

Table 3: Isotope data for clay, silt, and gravel fractions of core samples.....31

LIST OF FIGURES

Page

Figure 1: Location of the study area 2

Figure 2: Thermal fields and geologic structures 6

Figure 3: Detailed map of the hydrothermal features for the EETF 8

Figure 4: Detailed map of the hydrothermal features for the CETF 10

Figure 5: Geologic map of Uzon 12

Figure 6: Various hydrothermal features of the Uzon Caldera 14

Figure 7: δD vs. $\delta^{18}O$ diagram of water samples 23

Figure 8: δD vs. $\delta^{34}S$ diagram of water samples 25

Figure 9: $\delta^{34}S$ values of minerals separated from core samples 32

Figure 10: $\delta^{34}S$ values vs. depth of minerals separated from core samples 34

Figure 11: δD vs. $\delta^{18}O$ diagram of acid-sulfate and meteoric water samples 37

Figure 12: δD vs. $\delta^{18}O$ diagram of alkali-chloride and meteoric water samples 40

Figure 13: Comparison of Uzon Caldera $\delta D/\delta^{18}O$ values vs. other hydrothermal systems 44

Figure 14: Schematic of the fractionation model 49

Figure 15: Spatial distribution of aqueous sulfate $\delta^{34}S$ values for the CETF 56

Figure 16: Spatial distribution of aqueous sulfate $\delta^{34}S$ values for the EETF 58

Figure 17: $\delta^{34}S$ values of the various S-bearing species collected from vapor vs. liquid-dominated environments. 61

CHAPTER 1: INTRODUCTION

The Uzon Caldera is an active epithermal system located on the east coast of the Kamchatka Peninsula, roughly 180km north of the main shipping port Petropavlosk-Kamchatsky (Fig. 1). The caldera, along with its neighboring system Geyser Valley, has been protected as part of the Kronotsky State Biospheric Preserve since 1882 (Karpov, 1998). As a result of the protection of the preserve and the remote location, the caldera and surrounding areas have remained pristine, providing a unique opportunity for scientists of all fields to conduct interdisciplinary research. With funding provided by NSF, an international Microbial Observatory has been established that supports projects focusing on the microbiological, hydrological, and geological systems in order to utilize this opportunity.

In this paper we present the results of a chemical and isotopic study of the various waters present within the Uzon Caldera, as well as sulfur bearing minerals from within and around hydrothermal discharges, fumaroles, and sulfidized/acid-sulfate altered outcrops. These data are used in conjunction with modeling to constrain the origin of chemical components, and to characterize the geochemical, biological, and hydrological processes that produce the observed chemical/isotopic signatures and surface distribution of the various water types and mineralizations found throughout the active hydrothermal system.

1.1: Regional Geology

The Kamchatka Peninsula is the northern continuation of the Kurile- Kamchatka volcanic arc. Recent hydrothermal activity on the peninsula has been divided into two zones, the Central Kamchatka volcanic zone and the East Kamchatka volcanic zone (Fig. 1). Although volcanic activity persists only in the east, collectively both zones are associated with over 130 different groups of active thermal springs (Karpov and Naboko, 1989.) The Semyachik geothermal region, of which the Uzon Caldera is a part, belongs structurally to the central part of the Eastern Kamchatka graben-syncline. The hydrothermal systems in this region are regionally controlled by two major fault zones. A northeast-trending zone of crustal extension 20 km wide known as the Volcanic Wide-Separation fault (VWS Fault) and a 5-6 km

Fig. 1. Location of the study area: (a) The Kamchatka Peninsula of Far-East Russia showing the Central and Eastern Volcanic Zones; (b) Map with location of the Uzon Caldera and surrounding calderas, as well as the major regional faults; (c) The Uzon Caldera showing local faults and field/sample site locations (modified from O. A. Braitseva et al., 1974).

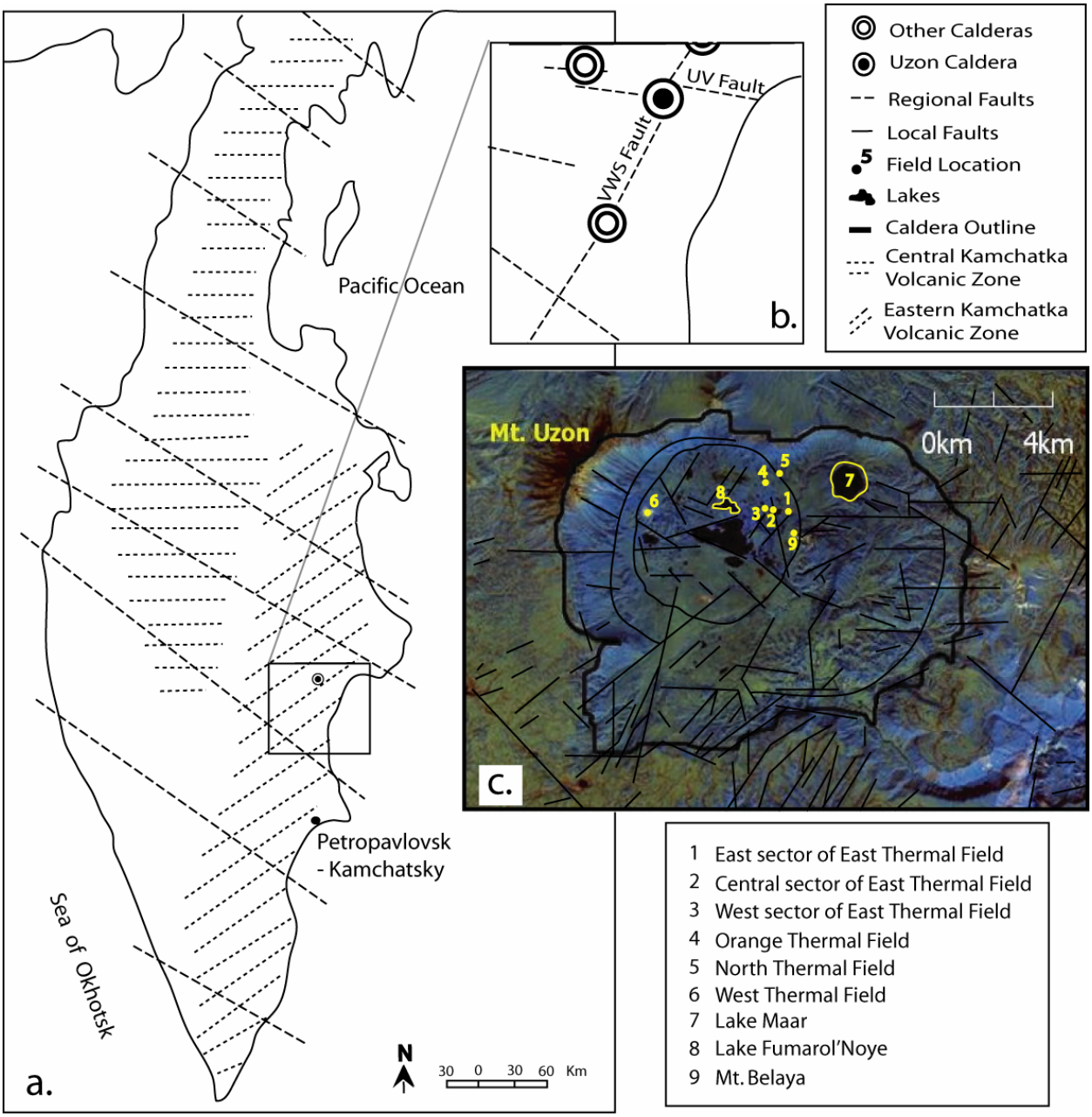
Other Calderas
Uzon Caldera
Regional Faults
Local Faults
Field Location
Lakes
Caldera Outline
Central Kamchatka Volcanic Zone
Eastern Kamchatka Volcanic Zone
Pacific Ocean
Sea of Okhotsk
Petropavlovsk - Kamchatsky
a.
b.
UV Fault
VWS Fault
c.
Mt. Uzon
0km
4km
1 East sector of East Thermal Field
2 Central sector of East Thermal Field
3 West sector of East Thermal Field
4 Orange Thermal Field
5 North Thermal Field
6 West Thermal Field
7 Lake Maar
8 Lake Fumarol'Noye
9 Mt. Belaya
N
30 0 30 60 Km

wide belt of sublatitudinal faults (trending 280) known as the Uzon-Valaginskii fault (UV Fault)(Fig 1). The point of intersection between these two faults plays an important part in channeling the majority of the Uzon caldera's thermal fluids to the surface (Belousov et al. 1984.)

1.2 Geologic History of Uzon

The Uzon caldera became volcanically active ca. 370-750 thousand years ago, beginning with the formation of a large shield volcano with a basement diameter of roughly 25km composed of olivine-two pyroxene and pyroxene-plagioclase basalts. In the middle Pleistocene a conic stratovolcano began to emerge on the shield volcano's western shoulder with a composition analogous to the previous basalts with only slightly lower silica and alkalinity values (Karpov, 1998). During Mid through Late Pleistocene, the Uzon volcanic structure underwent a series of eruptions that resulted in the discharge of 25×10^{10} tonnes of acidic pyroclastics and ignimbrites, which was quickly followed by an ejection of roughly 10×10^{10} tonnes of ash-pumice material. This consequently led to the final collapse of the chamber roof and formation of a ring fault system about 40,000 years ago, thus forming the Uzon Caldera (Karpov and Naboko, 1989.) A quiet period then ensued where a large lake basin developed within the caldera's depression.

Near the end of the Late Pleistocene, roughly 10-12 thousand years ago, resurgent activity in the east southeast section of the caldera resulted in the formation of the Mt. Belaya dacite extrusive dome. Formation of a large maar of andesitic composition in the northeast corner of the caldera during the Holocene marks the most recent volcanism for the caldera (Karpov, 1998)(Karpov and Naboko, 1989).

Currently, the caldera shares an asymmetric oval shaped volcano-tectonic depression with a neighboring river valley to the east known as Geysernaya river valley (Karpov, 1995). Part of the extinct stratovolcanic cone now refered to as Mt. Uzon, as well as the adjacent north and west walls, are the only topographic indications of the caldera rim to have survived chamber collapse and subsequent erosion. Where ring fractures associated with the collapse intersect the NE trending minor faults and deep

sublatitudinal regional faults, circulating hydrothermal fluids have been channeled to the surface forming the spatial pattern of the hydrothermal fields seen today (Fig. 1).

1.3 The Hydrothermal System of Uzon

Six active thermal fields within the caldera are the focus of this study, including the East sector of the East Thermal Field (EETF), the Central sector of the East Thermal Field (CETF), the West sector of East Thermal Field (WETF), the West Thermal Field (WTF), the Orange Thermal Field (OTF), and the North Thermal Field (NTF). Samples were also collected from a remnant hot spring system on the flank of the Mount Belaya resurgent dome complex, the Holocene Lake Dal'nee, and thermal Lake Fumarol'Noye (Figs. 1 through 4).

For the last 40 Ka, sediment has been transported from the caldera margins and deposited in lacustrine environments forming a thick "gravellite" substrate through which thermal fluids for several of the active low lying fields (EETF, CETF, OTF) ascend (Karpov and Naboko, 1990). Fluids in the higher elevation hydrothermal fields along the northern and western margins of the caldera (NTF, WTF) ascend through coarser alluvial/talus-slope sediment derived from the dacitic tuff-lava sequences rimming the caldera. In the case of the WTF, glacial sedimentation may have also played a part in sediment deposition (Belousov et al., 1984). All other lithologies, although relevant for the geologic history of the Uzon, are limited to maps and illustrations for completions sake rather than significance to this paper (Fig 5).

Within the active thermal fields, a variety of springs, pools, mud volcanoes, mudpots, and lakes dot the surface (Fig. 6 a-h). Depending upon the average precipitation for the year and the particular season, pool and thermal lake sizes fluctuate widely due to the low, flat topography within the majority of the caldera. In most cases, the thermal lakes and pools remain fixed in position and dimension. A mixture of gases composed predominately of H_2O and CO_2, with lesser H_2S, H_2, NH_3, CH_4, CO, and N_2, stream to the surface transporting chemical components as well as heat (Dymkina, Solomonov, Karpov, 1988; Karpov 1998). This very energetic gas release gives waters the appearance of boiling, yet

Fig. 2. Various thermal fields and geologic structures of the Uzon Caldera: (a) Aerial view of the Eastern Sector of East Thermal Field looking NW with Bannoe and Sulphur Lakes to the far right; (b) The Central Sector of East Thermal Field looking W with Kloridnoe Lake in the foreground; (c) The West Thermal Field looking SW; (d) Mount Belaya looking SE with part of the East Sector of East Thermal Field in the foreground; (e) Aerial view of the Lake Dal'nee maar looking NE.

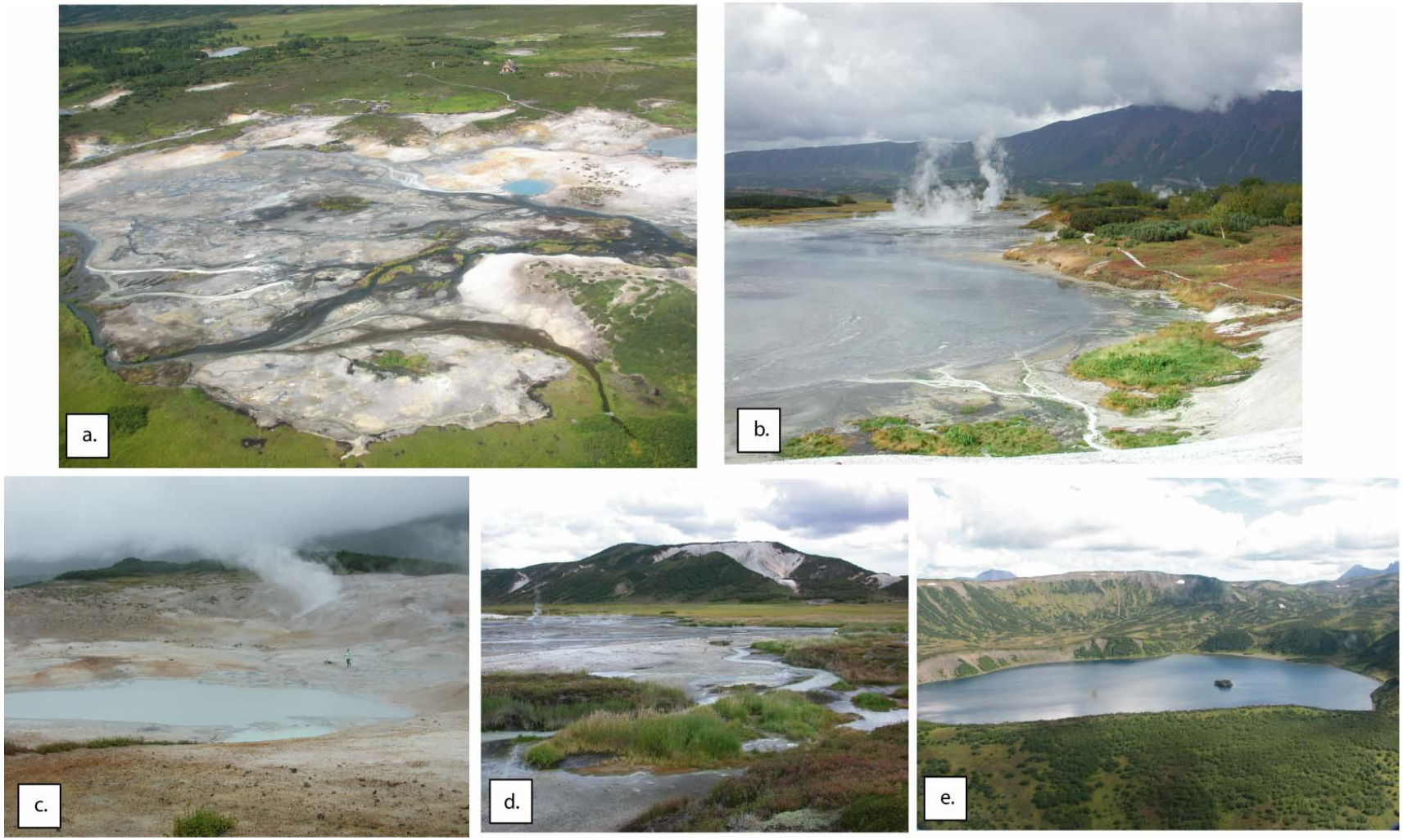
a.
b.
c.
d.
e.

Fig. 3. Detailed map of the hydrothermal features for the EETF showing the location of water, rock, and core sample sites.

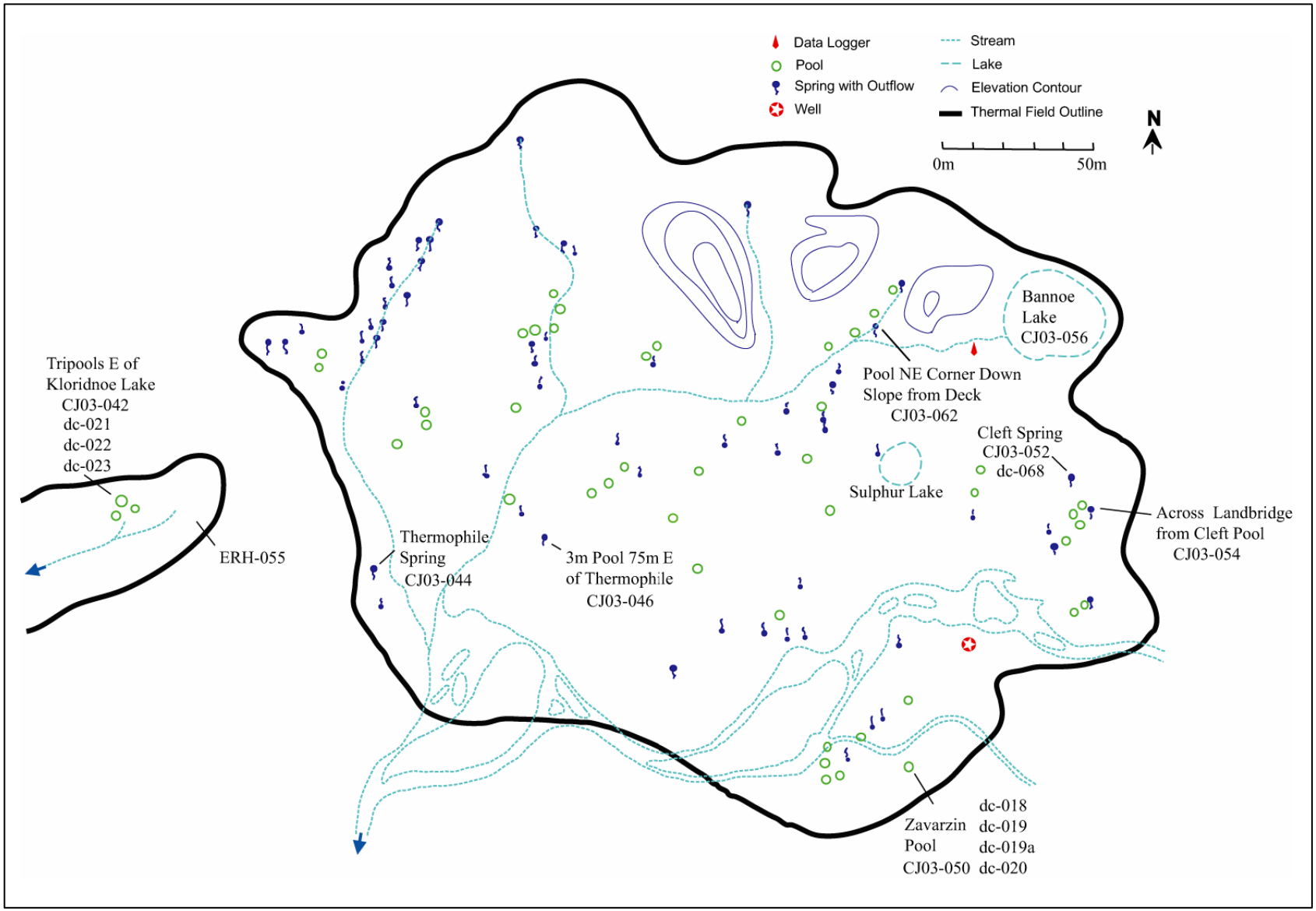
Data Logger
Pool
Spring with Outflow
Well
Stream
Lake
Elevation Contour
Thermal Field Outline
0m
50m
N
Tripools E of
Kloridnoe Lake
CJ03-042
dc-021
dc-022
dc-023
ERH-055
Thermophile
Spring
CJ03-044
3m Pool 75m E
of Thermophile
CJ03-046
Bannoe
Lake
CJ03-056
Pool NE Corner Down
Slope from Deck
CJ03-062
Cleft Spring
CJ03-052
dc-068
Sulphur Lake
Across Landbridge
from Cleft Pool
CJ03-054
Zavarzin
Pool
CJ03-050
dc-018
dc-019
dc-019a
dc-020

Fig. 4. Detailed map of the hydrothermal features for the CETF showing the location of water, rock, and core sample sites.

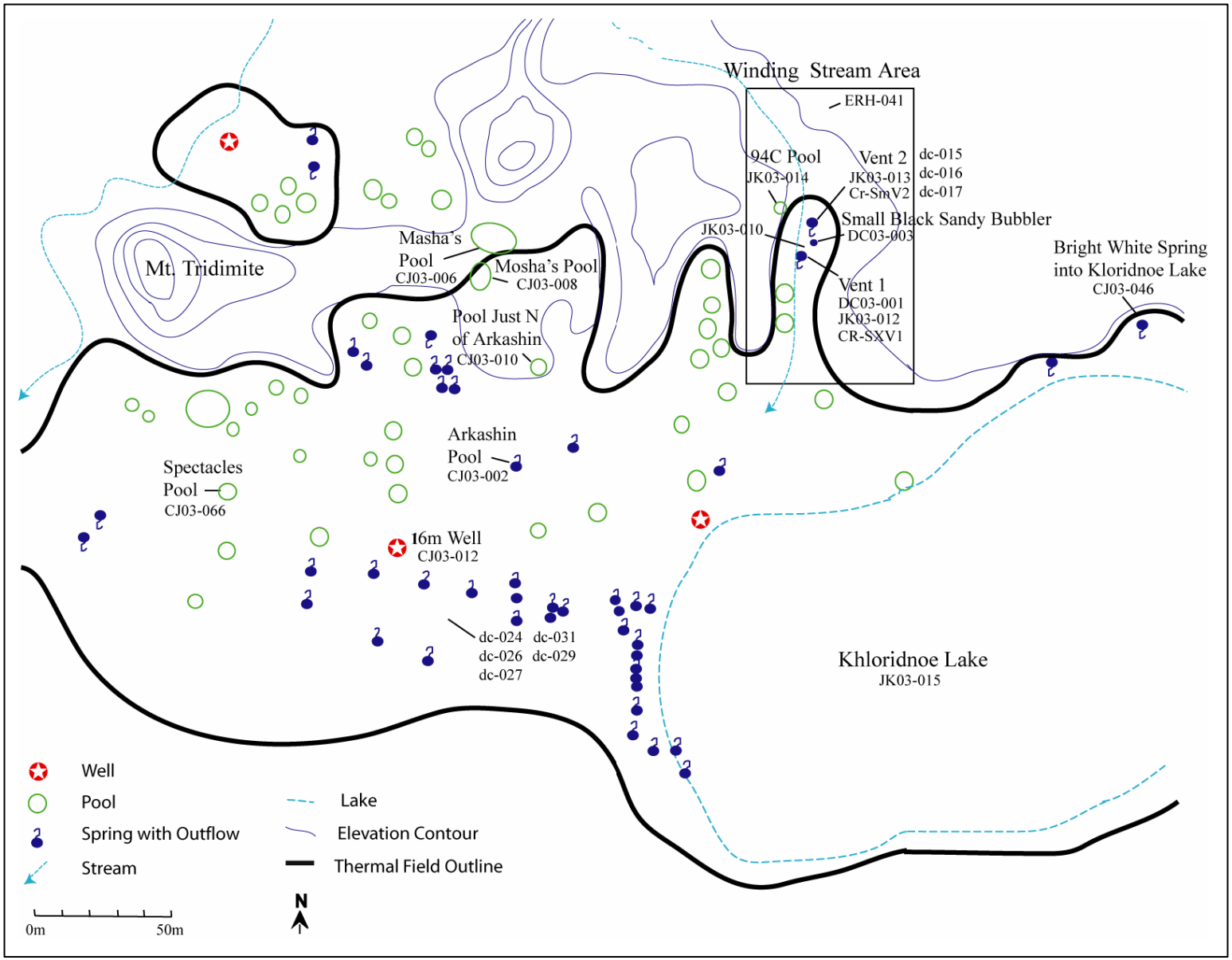
Winding Stream Area
ERH-041
94C Pool
JK03-014
Vent 2
JK03-013
Cr-SmV2
dc-015
dc-016
dc-017
Small Black Sandy Bubbler
DC03-003
JK03-010
Vent 1
DC03-001
JK03-012
CR-SXV1
Bright White Spring
into Kloridnoe Lake
CJ03-046
Mt. Tridimite
Masha's
Pool
CJ03-006
Mosha's Pool
CJ03-008
Pool Just N
of Arkashin
CJ03-010
Arkashin
Pool
CJ03-002
Spectacles
Pool
CJ03-066
16m Well
CJ03-012
dc-024
dc-026
dc-027
dc-031
dc-029
Khloridnoe Lake
JK03-015
Well
Pool
Spring with Outflow
Stream
Lake
Elevation Contour
Thermal Field Outline
N
0m
50m

Fig. 5. Geologic map of the Uzon-Geyser depression (modified from Braitseva et al., 1974).

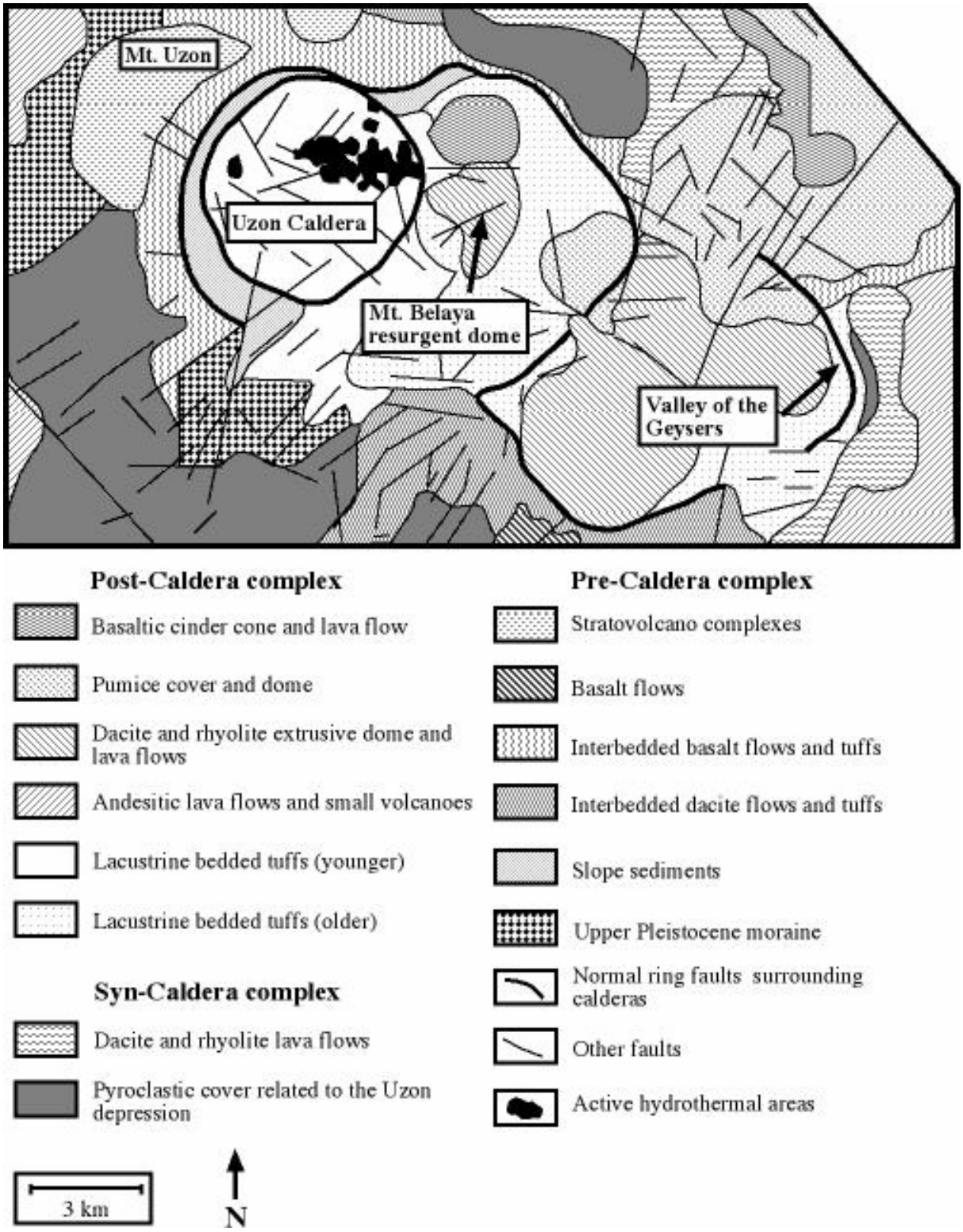
Mt. Uzon
Uzon Caldera
Mt. Belaya resurgent dome
Valley of the Geysers
Post-Caldera complex
Basaltic cinder cone and lava flow
Pumice cover and dome
Dacite and rhyolite extrusive dome and lava flows
Andesitic lava flows and small volcanoes
Lacustrine bedded tuffs (younger)
Lacustrine bedded tuffs (older)
Syn-Caldera complex
Dacite and rhyolite lava flows
Pyroclastic cover related to the Uzon depression
Pre-Caldera complex
Stratovolcano complexes
Basalt flows
Interbedded basalt flows and tuffs
Interbedded dacite flows and tuffs
Slope sediments
Upper Pleistocene moraine
Normal ring faults surrounding calderas
Other faults
Active hydrothermal areas
3 km
N

Fig. 6. Various pools, springs, mudvolcanoes, mudpots, wells, and sulfur bearing samples of the Uzon Caldera: (a) Arkashin pool (CETF); (b) unnamed spring (EETF); (c) Thermophile spring (EETF); (d) Zavarzin pool (EETF); (e) Spectacles pool (CETF); (f) Recently erupted mudvolcano (CETF); (g) Bubbling mudpot (CETF); (h) 16m well (CETF); (i) Core sample showing amorphous to crystalline As ore mineralization (CETF); (j) Core sample (Zavarzin) showing sulfur to pyrite redox gradient (EETF); (k) "Gravellite" cemented by amorphous As sulfide and S mineralization (CETF); (l) Sulfur crystals couating a sinter deposit (CETF Winding Stream Area).


a.


b.


c.


d.


e.

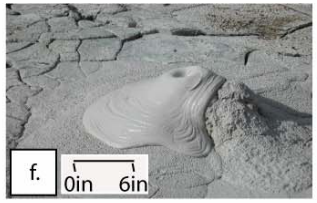
f.
0in
6in

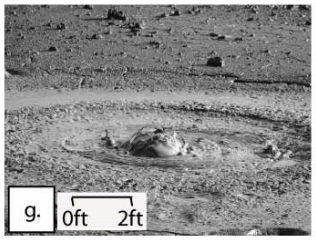
g.
0ft
2ft


h.


i.


j.


k.
0ft
3in


l.

temperatures measured at the surface never exceed 100°C. Field evidence suggests a history of high-temperature, phreatic explosive events for most of the thermal fields (Karpov, 1998; Eroshchev-Shak, Karpov, Il'in, 1985). Phreatic explosions as recent as 1989 attest to the continuation of this process in shaping the surface of the caldera (Karpov, 1998).

Various sulfur-bearing mineral phases are found across the surface of Uzon occurring either as minerals precipitating from vapor or vapor condensation, acid sulfate alteration products, or as aqueous phase precipitates within the sediment around hydrothermal discharges (Fig. 6 i-l). The most notable example of aqueous phase precipitation is that of an actively mineralizing As-Sb-Hg ore zone forming within the top two meters of the CETF (Migdisov et al., 1992). Also of interest is the presence of a molten sulfur layer, usually associated with active crater lakes, found forming a false bottom (depth of 26.5m) in Lake Bannoe, one of the EETF's larger pools (Karpov, 1998).

Although the last magmatic eruption occurred during the Holocene, possible influx of magma into a shallow chamber beneath the caldera has been detected by a recent Satellite Interferometric Synthetic Aperture Radar (InSAR) survey (Pritchard and Simons, 2004). Although limited by only a few measurements, the survey revealed inflation within the caldera of ~1.5cm/yr LOS. Best fit models designed to calculate the depth of the inflation source suggest a magma chamber depth that correlates with the already identified 5 km deep chamber located by geophysical data (Waltham, 2001). This continued shallow influx of magma confirms that the source of heat fueling the convective processes within the caldera (and thus the majority of the chemical components cycling in the subsurface) is magmatic in origin.

CHAPTER 2: METHODS

2.1 Field Methods

Water samples were collected from various springs, pools, and mudpots. Water was also collected from a steam well cased at 16m within the CETF. When possible, pH and temperature measurements were made. Due to the prolific bacterial growth within Uzon's aqueous environments, particular attention was paid to sampling processes that minimized undue chemical and/or isotopic exchange activity via metabolic processes. Samples for elemental analysis were acidified with HNO_3 to prevent subsequent precipitation after collection. For storage, refrigeration was used.

Rocks and sediments were collected from outcrops, fumaroles, and crusts/sinters within and around hydrothermal discharges. The focus of the collection process was on any material that potentially contained sulfur-bearing minerals. Core samples were extracted from within and adjacent to several pools using a 3 inch diameter clear PVC pipe. The core was subdivided according to textural and mineralogical differences, and placed into separate sterile plastic bags for transport and storage. Refrigeration was used to prevent further microbial activity.

2.2 Lab Methods

Water:

Acidified water samples were sent to the Chemical Analysis Laboratory at the University of Georgia for ICP-MS analysis using a VG Inductively Coupled Plasma Mass Spectrometer. Twenty-three elements were analyzed using this process. Standard error is less than 5%.

Inorganic anion analysis was performed at the Savanah River Ecology Lab on a DX-500 ion chromatography system with a Thermo AS3500 automated sampler. Separation was achieved on an AS4A-SC anion exchange column with 0.18 M sodium carbonate/0.17 M sodium bicarbonate eluent under 7 psi N_2 at a flow rate of 2ml/min with an injection volume of 20 µl at room temperature (Dionex Corp).. Anions were detected by CD20 Conductivity Detector with ASRS Ultra II eluent suppression at 50 mA current (Dionex Corp). Anion identities were assigned by comparison to

retention times of known standards, consistent with U.S. EPA Method 300.0. Concentrations are reported in mg/L with a 0.26 standard deviation.

For aqueous sulfate extraction, both the acidified and unacidified splits were analyzed (Appendix A). After each sample was filtered, a 10% $BaCl_2$ solution was added. The resulting $BaSO_4$ precipitate was washed, dried, and saved for S isotope analysis.

Handsamples:

For those samples containing identifiable and easily separable crystalline sulfide or elemental sulfur minerals, the individual S-bearing minerals were hand picked under a binocular scope and saved for S isotope analysis. All other rock material was prepared for mineralogical analysis using techniques detailed by Moore and Reynolds (1997) and analyzed using a Scintag X-ray Diffractometer at the University of Georgia Geology Department. Identified S-bearing minerals were saved for S isotope analysis.

Core Sediments:

Each core sample was size fractionated into sand, silt, and clay sized material using sieves and an IECB-22M high speed centrifuge at the University of Georgia Geology Department.

The gravel sized fraction was inspected for any S bearing minerals under a binocular scope, and these minerals were hand picked and saved for S isotope analysis. The silt size and clay size fractions were prepared for XRD for mineralogical analysis according to techniques detailed by Moore and Reynolds (1997). Coexisting pyrite and elemental sulfur were separated via heating to 150°C for 24 h to remove elemental sulfur by sublimation. Upon cooling, the remaining pyrite was removed and saved for isotopic analysis.

Stable Isotopes:

The $\delta^{18}O$ of waters was measured using a modified CO_2-water equilibration technique (Epstein and Mayeda, 1953; Socki et al, 1992). A Finnigan GasBench II peripheral device connected to a Finnigan Delta^{Plus} XL mass spectrometer was used for all isotope ratio measurements. All samples

were analyzed in continuous flow mode. Standards include DITAP and NIST reference material # VSMOW. Isotopic ratio results are reported in standard delta notation relative to VSMOW with a 2σ standard deviation of ±0.1‰. Measurements were made at SREL.

The δD of waters was measured using a Finnigan TC-EA peripheral device connected to a Finnigan Delta^{Plus} XL CF-IRMS. The DITAP and VSMOW standards were used for calibration. Isotope ratio results are reported relative to VSMOW and have a 2σ standard deviation of ±1.5‰. Analyses were performed at SREL.

$\delta^{34}S$ analysis for all S-bearing minerals was performed at the University of Georgia Geology Department's Stable Isotope Laboratory. All minerals were reacted with V_2O_5 at 1100°C to produce SO_2 gas. The SO_2 was analyzed by a Finnigan-MAT 253 gas source mass spectrometer using a dual inlet. Standard reference materials, including NZ-1, NBS-127, NBS-123, and Soufre De Lacq, were run to calibrate $\delta^{34}S$ values to the Canyon Diablo Troilite. Isotope ratio results have a 2σ ±0.4‰ standard deviation.

CHAPTER 3: RESULTS

3.1 Water Chemical, δD, $\delta^{18}O$, and $\delta^{34}S$ Isotope Geochemistry

Field measurements and analytical results from water samples taken at springs, pools, thermal lakes, wells, mudpots, and streams are reported in Table 1. Highlighted values represent anomalously high concentrations of elements with respect to local meteoric groundwaters.

Elemental and pH Data

Three types of thermal waters have been identified on the basis of elemental and pH data including: 1) an acid-sulfate water 2) an alkali-chloride water and 3) a mixing product resulting from varying degrees of dilution of the alkali-chloride water with meteoric surface water, which will be referred to as the dilute mixed waters throughout this paper. Included as a subgroup of the dilute mixed waters is a group of pools with anomolously high Li values referred to as the high Li dilute mixed waters.

The waters from the higher elevation, peripheral WTF, as well as from the more centrally located OTF, are chemically similar to acid-sulfate spring systems described by Goff et al. (1985) and White et al. (1971). Chloride is generally less than 20ppm, the dominant anion is SO_4^{-2}, pH is low, and concentrations of Fe, Al, Ca, Mn and Mg are significantly elevated with respect to Na and K. Trace-elements such as Li and B, as well as most heavy metals, are found only in low concentrations, although they are higher than background values for the cold surface meteoric waters. Additionally, these acid-sulfate waters contain anomalous concentrations of P, and in the case of the WTF, As and Sb.

In the lower elevation fields (CETF, EETF, and Lake Fumarol'Noye), water chemistries of the alkali-chloride springs are in sharp contrast with those of the acid-sulfate. These waters are compositionally similar to those alkali-chloride waters described by Goff et al. (1985), where Cl^- is the dominant anion with SO_4^{-2} occurring only in minor concentrations, pH is generally circum-neutral, and contents of Na and K are greatly elevated with respect to Al, Fe, Mn, Ca, and Mg. Trace-elements

Table 1
Chemical and stable isotope data for water samples taken from various pools, springs, wells, thermal lakes, mudpots and streams of Uzon Caldera. Underlined values represent anomalous concentrations of elements with respect to local meteoric groundwaters.

Sample no.	Sample Name	Location[cd]	Ph	Temp (°C)	Ag (ppb)	Al (ppm)	As (ppm)	B (ppm)	Ba (ppm)	Ca (ppm)	Cu (ppb)	Fe (ppm)	K (ppm)	Mg (ppm)	Mn (ppm)	Na (ppm)	P (ppm)	Pb (ppb)	Sb (ppm)	Si (ppm)	Sr (ppb)	Zn (ppb)	Li (ppb)	Au (ppb)	Hg (ppb)	SO4 (ppm)	Cl (ppm)	Water $\delta^{18}O$ (‰)	Water δD (‰)	Sulfate $\delta^{34}S$ (‰)
Acid Sulfate Waters																														
DC03-007	Small Easternmost Pool	WTF	2.60	73.00	0.01	94.99	1.39	0.06	0.03	11.86	0.04	83.68	1.81	11.08	0.55	6.06	1.05	0.39	0.92	117.40	0.05	0.08	3.00	-	-	1777.25	4.00	-2.30	-78.24	0.30
CJ03-022	Mud Pot	OTF	2.40		0.02	115.30	1.82	0.96	0.03	38.62	0.04	72.72	7.39	28.37	1.94	23.48	1.81	0.52	0.76	93.87	0.09	0.56	28.86	7.59	-	2373.61	7.00	-6.84	-94.16	-1.20
CJ03-062	Pool NE Corner Down Slope from Deck	EETF																								504.00	26.00	-6.84	-93.81	
DC03-005	Lowermost Large Pool	WTF	2.60	33.00	0.02	311.40	4.40	0.28	0.03	56.23	0.13	424.30	1.96	43.16	2.62	5.12	3.65	1.16	2.57	109.60	0.06	0.44	9.22	-	-	3439.86	20.00	-8.74	-96.95	0.20
DC03-012	Very Active High Temp Vent	WTF	3.10		0.02	93.04	1.50	0.88	0.03	28.18	0.07	203.20	3.72	16.06	1.02	13.91	1.24	0.43	1.10	64.57	0.08	0.43	6.79	-	-	3368.78	23.00	-7.17	-84.47	0.00
CJ03-020	Center Pool	OTF	6.60		0.02	15.66	0.50	0.24	0.02	2.85	0.01	5.72	1.89	1.27	0.06	3.64	0.36	0.16	0.13	39.94	0.01	0.06	0.70	-	3.53	768.59	3.00	-2.32	-74.66	-0.30
CJ03-008	Masha's pool	CETF	2.50	82.00	0.02	39.72	0.88	1.77	0.03	17.06	0.04	32.70	7.76	8.70	0.73	28.51	0.69	0.27	0.31	150.00	0.04	0.35	35.48	-	-	730.84	36.00	-9.57	-97.33	-0.10
CJ03-006	Masha's Pool	CETF	2.60	50.00	0.02	15.80	0.59	9.83	0.06	75.29	0.07	11.79	14.91	32.60	2.14	120.30	0.49	0.20	0.22	150.90	0.25	2.65	151.98	3.24	-	625.24	68.00	-6.27	-87.42	-0.20
CJ03-010	Pool Just N of Arkashin	CETF	2.60	66.00	0.02	18.73	0.96	10.40	0.02	50.35	0.03	39.75	9.65	18.43	1.20	152.70	0.58	0.20	0.18	119.00	0.03	0.25	639.75	3.84	-	641.35	254.00	-9.77	-100.33	0.00
CJ03-018	Clear Pond Across Orange Island	OTF	2.50		0.02	15.70	0.83	17.54	0.04	18.57	0.02	11.21	11.96	2.65	0.19	243.10	0.52	0.15	0.22	70.65	0.07	0.05	135.64	4.66	-	744.52	397.00	-6.70	-87.55	-0.30
Alakli-Chloride Waters																														
CJ03-058	Fumarol'Noye Lake	LFN			-	0.18	2.56	31.39	0.03	18.93	-	0.07	75.35	0.54	0.04	586.20	0.02	-	0.66	72.84	0.34	0.01	5369.70	-	-	61.33	1090.00	-11.43	-104.37	
CJ03-012	16 M Well	CETF	4.80	100.00	0.02	0.12	6.66	76.73	0.03	54.51	0.04	1.28	125.30	2.45	0.42	1037.00	0.23	0.13	0.65	119.70	0.18	0.03	1406.00	24.58	-	97.07	2239.00	-10.58	-97.22	8.60
CJ03-002	Arkashin Pool	CETF	4.80	69.00	0.02	0.04	5.75	81.86	0.16	47.60	0.03	0.11	91.15	1.76	0.23	1269.00	0.28	0.14	0.76	118.40	0.19	0.11	1084.00	35.23	-	79.18	2398.00	-9.15	-100.24	7.60
CJ03-066	Spectacles Pool	CETF			-	0.06	5.53	73.94	0.17	49.47	-	0.05	83.89	1.40	0.43	1295.00	0.13	0.01	0.61	123.60	0.20	0.03	1090.30	72.34	3.00	109.66	2405.00	-8.16	-97.82	13.20
High Li Dilute Mixed Waters																														
CJ03-046	3m Pool 75m East of Thermophile Spring	EETF	4.50	80.00	0.01	0.46	0.32	18.21	0.06	33.44	-	0.10	18.86	1.58	0.43	229.70	0.10	0.03	-	102.80	0.12	0.04	1079.80	76.04	2.80	392.98	309.00	-6.02	-82.34	3.80
CJ03-004	Sunlight Spring	WETF	6.00	54.00	0.01	0.11	0.47	10.88	0.05	42.00	0.02	0.50	35.89	7.38	0.31	267.80	0.23	0.09	0.13	113.90	0.16	0.05	1085.10	9.09	-	98.44	350.00	-13.91	-109.86	
CJ03-042	Tripools East of Kloridnoe Lake	EETF	5.20	77.00	-	0.95	0.38	11.36	0.05	35.23	-	0.25	16.21	6.00	0.69	169.90	0.35	0.02	-	96.11	0.16	0.02	945.20	56.05	6.74	222.98	242.00	-8.67	-96.83	3.70
CJ03-014	Burlyashchy Spring	WETF			0.01	0.01	0.52	11.10	0.08	34.27	0.01	0.21	22.31	8.09	0.29	213.50	0.27	0.11	0.06	87.19	0.13	0.03	754.43	2.45	-	230.20	251.00	-7.94	-92.12	4.10
Dilute Mixed Waters																														
CJ03-056	Lake Bannoe	EETF	4.9[b]	41.9[b]	-	0.29	-	0.51	0.05	15.83	0.01	0.33	7.35	4.04	0.31	26.87	0.54	-	0.28	91.97	0.08	0.04	26.88	-	-	92.98	11.00	-14.81	-107.11	13.8[b]
CJ03-050	Zavarzin Pool	EETF	5.80	54.00	-	0.02	0.03	0.72	0.05	19.93	0.01	0.00	5.53	6.04	0.43	34.83	0.26	-	0.35	72.99	0.09	0.01	35.69	4.47	-	53.47	17.00	-14.20	-107.20	8.00
CJ03-048	Data Logger Pool near Lake Bannoe	EETF	5.80		0.01	0.01	0.37	10.17	0.01	26.78	-	-	10.63	1.33	0.13	167.20	0.12	0.03	-	97.68	0.07	0.01	721.37	42.35	-	130.30	64.00	-11.20	-96.28	6.20
CJ03-054	Across Land Bridge from Cleft Spring	EETF	4.80		-	0.98	-	0.19	0.07	29.60	0.02	0.12	3.98	3.89	0.51	24.13	0.33	-	0.35	67.67	0.12	0.02	13.42	-	-	161.66	4.00	-12.09	-100.46	1.90
CJ03-052	Cleft Spring	EETF	6.00		-	0.05	0.00	0.56	0.04	27.72	0.04	0.01	7.62	2.72	0.23	43.60	0.05	-	0.40	92.81	0.11	0.00	46.22	19.29	-	130.88	13.00	-12.90	-101.50	2.30
CJ03-028	Gray Filamentous Pool	NTF	5.80		-	0.01	0.01	1.02	0.05	15.29	0.01	0.08	11.01	1.97	0.25	28.32	-	-	-	69.66	0.08	0.01	14.22	106.85	-	40.18	31.00	-16.09	-119.34	
CJ03-026	Small Yellow Pond	NTF	5.80		-	0.26	0.02	0.94	0.22	32.96	0.03	0.41	14.50	7.02	0.62	40.61	0.20	0.03	-	116.30	0.18	0.03	14.37	26.60	-	132.69	35.00	-15.76	-115.24	
CJ03-064	Bright White Spring into Kloridnoe Lake	CETF	5.50		-	0.06	0.02	1.91	0.02	19.88	-	0.02	10.25	7.83	0.33	51.33	0.22	-	0.40	85.22	0.07	0.00	49.95	0.14	8.94	80.47	40.00	-15.47	-112.42	
DC03-003	Small Black Sandy Bubbler 8m N of Vent 1	CETF[a]	5.60	69-83	0.01	0.72	0.07	2.09	0.03	5.10	0.03	0.08	6.02	1.01	0.05	32.92	0.10	0.06	0.27	82.02	0.02	0.03	22.89	-	-	235.40	42.00	-8.88		3.40
CJ03-024	First Deep Blue Pool	NTF	5.00		0.03	-	0.02	1.75	0.07	21.55	0.03	0.02	15.63	2.77	0.38	43.18	0.19	0.03	-	100.30	0.12	0.04	23.65	219.99	-	21.09	56.00	-15.48	-112.63	
DC03-001	Vent 1	CETF[a]	5.50	85.00	0.01	0.13	0.10	4.06	0.08	20.81	0.01	0.03	13.44	5.76	0.60	75.95	0.32	0.05	0.27	126.80	0.06	0.03	119.44	10.18	12.17	123.54	76.00	-14.72	-110.61	4.20
JK03-012	Vent 1	CETF[a]	5.60	85.00	0.01	0.21	0.10	4.16	0.09	21.64	0.03	0.73	14.77	5.92	0.62	78.71	0.21	0.07	0.27	129.60	0.07	0.03	105.31	8.70	0.22	104.33	77.00	-14.51	-111.68	4.20
JK03-013	Vent 2	CETF[a]	5.50	80.00	0.01	0.18	0.09	5.09	0.09	28.01	0.00	0.37	16.60	3.81	0.61	91.88	0.20	0.07	0.23	138.60	0.09	0.02	100.25	5.14	-	164.28	87.00	-13.66	-106.35	2.80
CJ03-044	Thermophile Spring	EETF	4.40	75.00	0.02	-	0.15	5.32	0.06	34.15	-	-	15.44	11.12	0.60	131.10	0.38	0.02	-	109.40	0.15	0.00	444.34	97.70	0.28	19.91	90.00	-15.72	-111.70	
JK03-014	94°C Pool by Jen's Pools (same outflow)	CETF[a]	3.30	94.00	0.00	0.16	0.10	6.22	0.03	31.37	-	0.23	18.16	6.31	0.57	101.80	0.17	0.05	0.27	141.40	0.04	0.31	78.87	-	-	217.76	100.00	-14.41	-111.68	2.70
JK03-015	Kloridnoe Lake	CETF			0.00	0.77	0.35	12.78	0.07	27.50	0.00	1.02	22.04	6.80	0.53	221.80	0.32	0.05	0.27	99.53	0.11	0.05	-	-	-	185.24	305.00	-12.88	-106.59	3.80
Meteoric Waters																														
CJ03-032	WOR Stream	STM	7.10		-	-	-	-	0.00	2.75	0.02	0.03	-	0.64	0.00	4.03	0.05	-	-	17.36	0.00	0.06	1.90	-	-	1.43	0.00	-15.72	-110.33	
CJ03-036	Maar Lake Dal'nee	LMR	7.30		-	-	-	-	0.00	1.05	-	0.01	-	0.30	0.00	1.35	-	-	-	2.90	0.00	0.02	-	-	-	0.02	1.00	-14.08	-105.32	
CJ03-040	Stream Parallel to Maar Rim	STM			-	0.01	-	-	0.00	3.88	-	0.05	0.23	1.32	0.00	3.65	0.04	-	-	20.21	0.01	0.02	6.07	-	-	0.02	1.00	-15.60	-111.01	
CJ03-038	Headwaters	STM	7.00		-	-	-	-	0.00	3.86	-	-	0.15	1.02	0.00	2.88	0.05	-	-	16.40	0.01	0.02	-	-	-	0.02	2.00	-16.23	-116.23	
CJ03-016	Stream Komariny (campsite)	STM	7.10		0.01	0.01	0.31	0.20	0.02	4.03	0.01	0.11	3.33	1.51	-	7.25	0.21	0.08	0.04	20.62	0.01	0.06	10.58	-	-	1.96	2.00	-15.85	-113.57	
CJ03-030	Stream Draining Mt. Belaya	STM			-	0.27	-	-	0.04	4.70	0.02	1.05	0.15	0.82	0.09	2.27	0.02	-	-	16.81	0.02	0.03	-	26.99	-	4.15	2.00	-15.82	-112.76	

[a] Samples from within Winding Stream sample area (Fig. 4.)
[b] Average of data from Kusakabe et al. (2000.)
[c] West Thermal Field (WTF); Orange Thermal Field (OTF); East sector of East Thermal Field (EETF); Central sector of East Thermal Field (CETF); West sector of East Thermal Field (WETF); Lake Fumarol'Noye (LFN); North Thermal Field (NTF); Meteoric Streams (STM); Maar Lake Dal'nee (LMR.)
[d] See Fig. 1 for the location of samples from the WTF, OTF, WETF, LMR, and LFN, Fig. 3 for the location of samples from the EETF, and Fig. 4 for the location of samples from the CETF.

such as Li, B, As, and Sb also occur in higher concentrations with respect to background values of cold surface waters.

Mixed waters are by far the most prevalent water being discharged at the surface of the caldera. They are found both along the margin of thermal fields where temperatures are typically low, as well as in the more centrally located high temperature zones of thermal fields. The only exception to this is the WTF, where all thermal waters are the acid-sulfate type. Mixed waters generally do not retain any of the elemental signatures inherited from the parent alkali-chloride thermal fluid, although exceptions do occur such as those containing high Li concentrations.

δD /$\delta^{18}O$ Values

In a plot of δD vs. $\delta^{18}O$, surface and thermal spring waters fall along a line between local meteoric waters (LMW) and the primary magmatic water box (Fig. 7). A number of observations regarding this distribution can be made, including:

1. Acid-sulfate waters of the WTF and OTF have the highest δD and $\delta^{18}O$ values.
2. Alkali-chloride waters of the EETF, CETF and Lake Fumarol'Noye, as well as the mixed alkali-chloride/meteoric waters of the EETF, WETF and CETF that retain high Li concentrations have moderately high δD and $\delta^{18}O$ values.
3. All other dilute mixtures with consistently low elemental concentrations, as seen in the CETF, EETF, and NTF, have low δD and $\delta^{18}O$ values.
4. The cold surface meteoric waters sampled from streams and Lake Dal'nee all cluster around the meteoric water line (MWL) as defined by Craig (1961). We assume these compositions characterize the local meteoric water, although slight variations occur.

$\delta^{34}S$ Values

Results of the aqueous sulfate $\delta^{34}S$ analyses are shown in a plot of $\delta^{34}S$ vs. δD (Fig. 8). A complete list of $\delta^{34}S$ analysis can be found in Appendix C. The following trends are observed:

Fig. 7. δD and $\delta^{18}O$ of water samples from the Uzon Caldera. Dashed line indicates the projected magmatic-meteoric mixing line along which the samples plot; solid line is the meteoric water line as defined by Craig (1961). Sample types are designated in Table 1 for each sample.

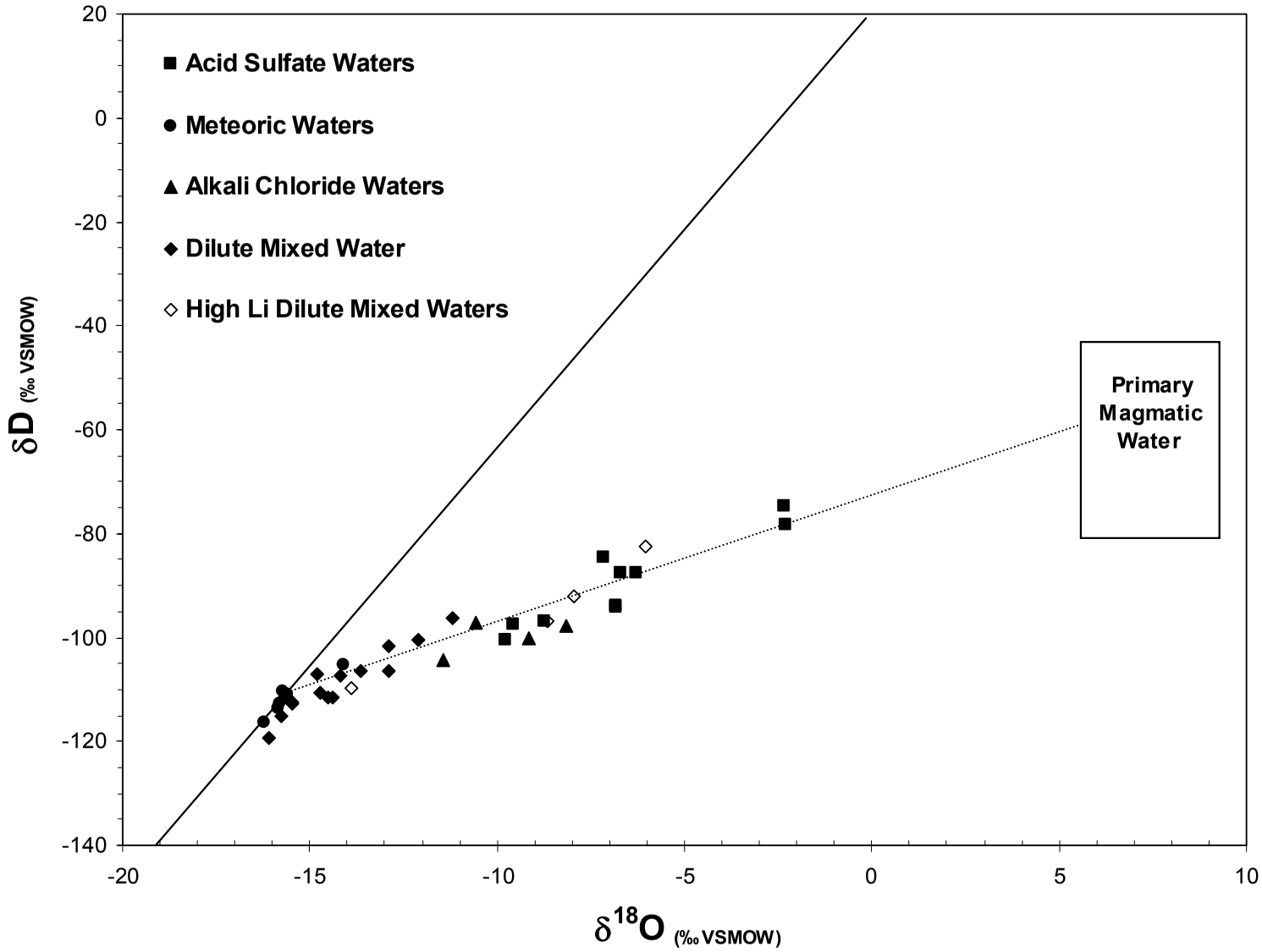
Acid Sulfate Waters
Meteoric Waters
Alkali Chloride Waters
Dilute Mixed Water
High Li Dilute Mixed Waters
Primary Magmatic Water
δD (‰ VSMOW)
δ18O (‰ VSMOW)
20
0
-20
-40
-60
-80
-100
-120
-140
-20
-15
-10
-5
0
5
10

Fig. 8. δD vs. $\delta^{34}S$ for thermal waters. Dashed vertical line shows the generally accepted $\delta^{34}S$ value for magmatic sulfur as a reference; solid horizontal line shows the calculated average δD for the local meteoric waters of Uzon as a reference.

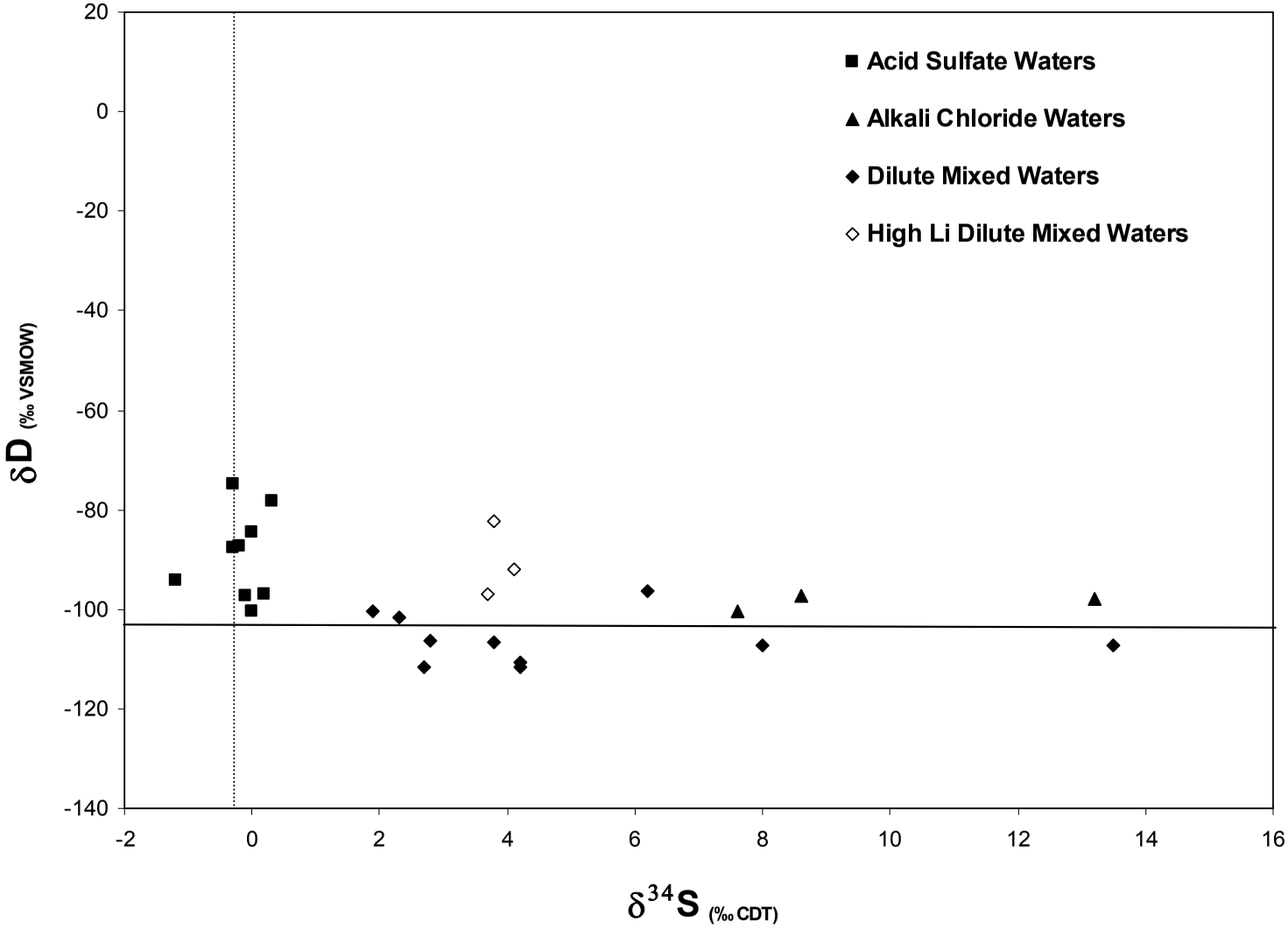
Acid Sulfate Waters
Alkali Chloride Waters
Dilute Mixed Waters
High Li Dilute Mixed Waters
δD (‰ VSMOW)
δ34S (‰ CDT)
20
0
-20
-40
-60
-80
-100
-120
-140
-2
0
2
4
6
8
10
12
14
16

1. Acid-sulfate type waters of the WTF and OTF have the lowest $\delta^{34}S$ values which all cluster at or below (0‰).

2. Alkali-chloride type waters of the EETF, CETF, and Lake Fumarol'Noye have the highest $\delta^{34}S$ values ranging from 7.6 to 13.2‰. Interestingly, two of the highly dilute mixed pools (Zavarzin and Bannoe Pool), neither of which show the elemental characteristics associated with the alkali-chloride type waters, display the same enriched isotopic signature.

3. The mixed waters of the EETF, WETF, and CETF that retain high Li concentrations have $\delta^{34}S$ values that fall within the 1.9 to 6.2‰ range displayed by the other highly dilute mixed waters with consistently low elemental concentrations.

4. The cold surface meteoric waters did not contain enough aqueous SO_4^{-2} for analysis in this study.

3.2 Mineral $\delta^{34}S$ Isotope Geochemistry

Fumarole Precipitate and Vapor Alteration Products

Results from the $\delta^{34}S$ analysis of minerals collected from in and around fumaroles and sulfidized/acid-sulfate altered outcrops are given in Table 2. Mineralogy of samples that required identification via XRD is shown in Appendix B along with characteristic XRD patterns. A complete list of $\delta^{34}S$ analyses can be found in Appendix C.

All minerals listed in Table 2 formed via H_2S oxidation from a vapor phase. Elemental sulfur forms directly from the hydrogen sulfide gas via the reaction (Seal et al., 2000):

$$H_2S_{(g)} + \tfrac{1}{2} O_{2(g)} \rightarrow S^0_{(s)} + H_2O_{(l)} \qquad (1)$$

A second possible reaction occurs during H_2S oxidation above the water table as follows:

$$H_2S_{(g)} + 2O_{2(g)} \rightarrow H_2SO_{4(l)} \qquad (2)$$

The resulting acid sulfate liquid condensate from equation 2 then reacts with calcic plagioclase within the steam heated andesitic host rock to form minamiite, a Ca-rich alunite group mineral (Celik, 1999).

Table 2
Sulfur isotope data for fumarole precipitates and vapor alteration minerals formed during the oxidation of H_2S.

Sample no.	Sample Name	Location[bc]	Sample Description	Mineral	$\delta^{34}S$ (‰)
Minerals From Active Areas					
CR-SXV1	Vent 1 Crystals[a]	CETF	Sinter Mineralization	S^0	+1.1
JK03-010	Near Outflow Channel[a]	CETF	Sinter Mineralization	S^0	+1.3
ERH-055	Tripool Area	EETF	Fumarole Precipitate	S^0	-1.5
ERH-052	WTF Sulfur	WTF	Fumarole Precipitate	S^0	+1.3
ERH-XTRA	West Slope of WTF	WTF	Vapor Alteration Min.	Minamiite	+1.6
ERH-041	Sulfidized Hillock[a]	CETF	Vapor Alteration Min.	S^0	+0.5
Minerals From Inactive Areas					
ERH-030-worwa	WOR Slope White	MTB	Vapor Alteration Min.	Minamiite	-5.1
ERH-030-worwb	WOR Slope White	MTB	Vapor Alteration Min.	Minamiite	-3.1
ERH-031-woro1	WOR Slope Orange	MTB	Vapor Alteration Min.	Minamiite	-0.4
ERH-031-woro3	WOR Slope Orange	MTB	Vapor Alteration Min.	Minamiite	-4.9
ERH-031-woro4	WOR Slope Orange	MTB	Vapor Alteration Min.	Minamiite	-3.4
ERH-032-worr1	WOR Slope Red	MTB	Vapor Alteration Min.	Minamiite	-5.2

[a] Samples from within Winding Stream sample area (Fig. 4).

[b] Central sector of East Thermal Field (CETF); East sector of East Thermal Field (EETF); West Thermal Field (WTF); Mount Belaya (MTB).

[c] See Fig. 1 for the location of samples from the WTF, Fig. 3 for the location of samples from the EETF, and Fig. 4 for the location of samples from the CETF.

All minerals collected from within the fumaroles and pool sinters are presumed to be actively precipitating from current H_2S gases, and have $\delta^{34}S$ values that range between -1.5 to +1.6‰ (Table 2). Sample erh-041 (the sulfur hillocks), although it no longer appears to be actively sulfidizing, was collected from an active hydrothermal area and is considered to have precipitated from gases isotopically similar to those currently depositing minerals.

The resurgent dome Mt. Belaya shows no current hydrothermal activity and is assumed to contain alteration minerals that reflect vapor compositions that exsolved during the early stages of the caldera's evolution. The $\delta^{34}S$ values of this latter group are depleted relative to current minamiite values, all lying within the -5.2 to -0.4‰ range.

Unfortunately, sampling of gas phases was not possible during this study. Instead, $\delta^{34}S$ analyses of the fumarole precipitate and vapor alteration minerals are used as proxies for the direct measurement of the $\delta^{34}S$ for the $H_2S_{(g)}$.

Sediment and Lithified Sediment

$\delta^{34}S$ data from core sediment and rock samples collected from within and around various pools are given in Table 3. The only the S-bearing minerals run for $\delta^{34}S$ analysis were the sulfides and elemental sulfur identified by XRD. Example XRD patterns, as well as a complete list of mineralogy for each core sub-sample can be found in Appendix B. A complete list of $\delta^{34}S$ isotope analysis can be found in Appendix C.

Figure 9 shows the $\delta^{34}S$ value and size fractions for various mineral separates. It appears that neither the mineral composition (ie. pyrite vs. realgar vs. sulfur) nor the size fraction (ie. >sand, silt, clay) of the sample is a factor in the degree of enrichment found between samples. The total range of values is ~7.5‰.

In order to determine whether $\delta^{34}S$ values are affected by depth within the core, and subsequently by any accompanying redox and/or temperature changes, a plot of the same samples grouped

according to the depth at which they formed is shown in Fig. 10. The only trend discernible is an apparent depletion in the overall range of $\delta^{34}S$ value of the minerals with increasing depth into the more reducing conditions.

Table 3
Sulfur isotope data for clay, silt, and gravel fractions of cores taken in and around various pools and mineralized zones.

Sample no.	Sample Name	Location[ab]	Horizon[c]	Depth (cm)	Size Fraction[d]	Mineral	$\delta^{34}S$ (‰)
dc03-018	ETF Zavarzin	EETF	a	4	Silt	S^0	+5.7
dc03-018	ETF Zavarzin	EETF	a	4	Clay	S^0	+0.2
dc03-019	ETF Zavarzin	EETF	b	10	Silt	S^0	-0.4
dc03-019a	ETF Zavarzin	EETF	c	16	Silt	Pyrite	+1.1
dc03-019a	ETF Zavarzin	EETF	c	16	Clay	Pyrite	+1.8
dc03-020	ETF Zavarzin	EETF	d	21	Silt	Pyrite	+0.7
dc03-021	ETF Tripool	EETF	a	4	Silt	S^0	+1.9
dc03-021	ETF Tripool	EETF	a	4	Clay	Pyrite	+3.8
dc03-022	ETF Tripool	EETF	b	8	Silt	S^0	+0.9
dc03-022	ETF Tripool	EETF	b	8	Clay	Pyrite	+3.4
dc03-023	ETF Tripool	EETF	c	15	Silt	S^0	+0.9
dc03-023	ETF Tripool	EETF	c	15	Clay	Pyrite	+1.3
dc03-068	ETF Cleft Bulk	EETF	bulk	5	Silt	Pyrite	0.0
dc03-068	ETF Cleft Bulk	EETF	bulk	5	Clay	Pyrite	+3.5
dc03-024	CTF Shovel	CETF	a	4	Silt	Pyrite	3.2
dc03-026	CTF Shovel	CETF	c1	9	Gravel	Realgar	+1.3
dc03-026	CTF Shovel	CETF	c1	9	Silt	Realgar	+2.4
dc03-027	CTF Shovel	CETF	c2	9	Silt	Realgar	+1.3
dc03-029	CTF 13 m SE K4	CETF	bulk	4	Gravel	Pyrite	+0.2
dc03-029	CTF 13 m SE K4	CETF	bulk	4	Silt	Pyrite	+1.5
dc03-029	CTF 13 m SE K4	CETF	bulk	4	Clay	Pyrite	+4.6
dc03-031	2m SW of shovel	CETF	b	13	Gravel	Pyrite	-0.1
dc03-015	CTF Jp vent[e]	CETF	a	2	Silt	S^0	+0.9
dc03-016	CTF Jp vent[e]	CETF	b	6	Silt	Pyrite	-0.6
dc03-017	CTF Jp vent[e]	CETF	c	12	Silt	Pyrite	-1.9
Cr-SmV2	Vent 2 JKpools[e]	CETF	bulk	4	Clay/Silt	S^0	-1.3
dc03-010	WTF sed/crust	WTF	bulk	5	Gravel	Pyrite	+0.9
dc03-010	WTF sed/crust	WTF	bulk	7	Clay	Pyrite	+0.9
ps04-029	OTF	OTF	c	8	Clay	Pyrite	+0.5

[a] West Thermal Field (WTF); Orange Thermal Field (OTF); East sector of East Thermal Field (EETF); Central sector of East Thermal Field (CETF); Lake Fumarol'Noye (LFN); North Thermal Field (NTF); Streams (STM); Maar Lake Dal'nee (LMR).

[b] See Fig. 1 for the location of samples from the WTF and OTF, Fig. 3 for the location of samples from EETF, and Fig. 4 for the location of samples from CETF.

[c] Horizons refer to the subdivided sections of the core distinguished visually using textural and mineralogical differences; a is the uppermost horizon, followed by b and c, with d being the deepest; c1 and c2 are verticalsplits within the same c horizon; bulk indicates no subdivision within the sample.

[d] Each subsample was size fractionated into its clay, silt, and gravel components.

[e] Samples from within Winding Stream sample area (Fig. 4).

Fig. 9. $\delta^{34}S$ values of minerals separated from core samples taken within and around springs and pools of the Uzon Caldera.

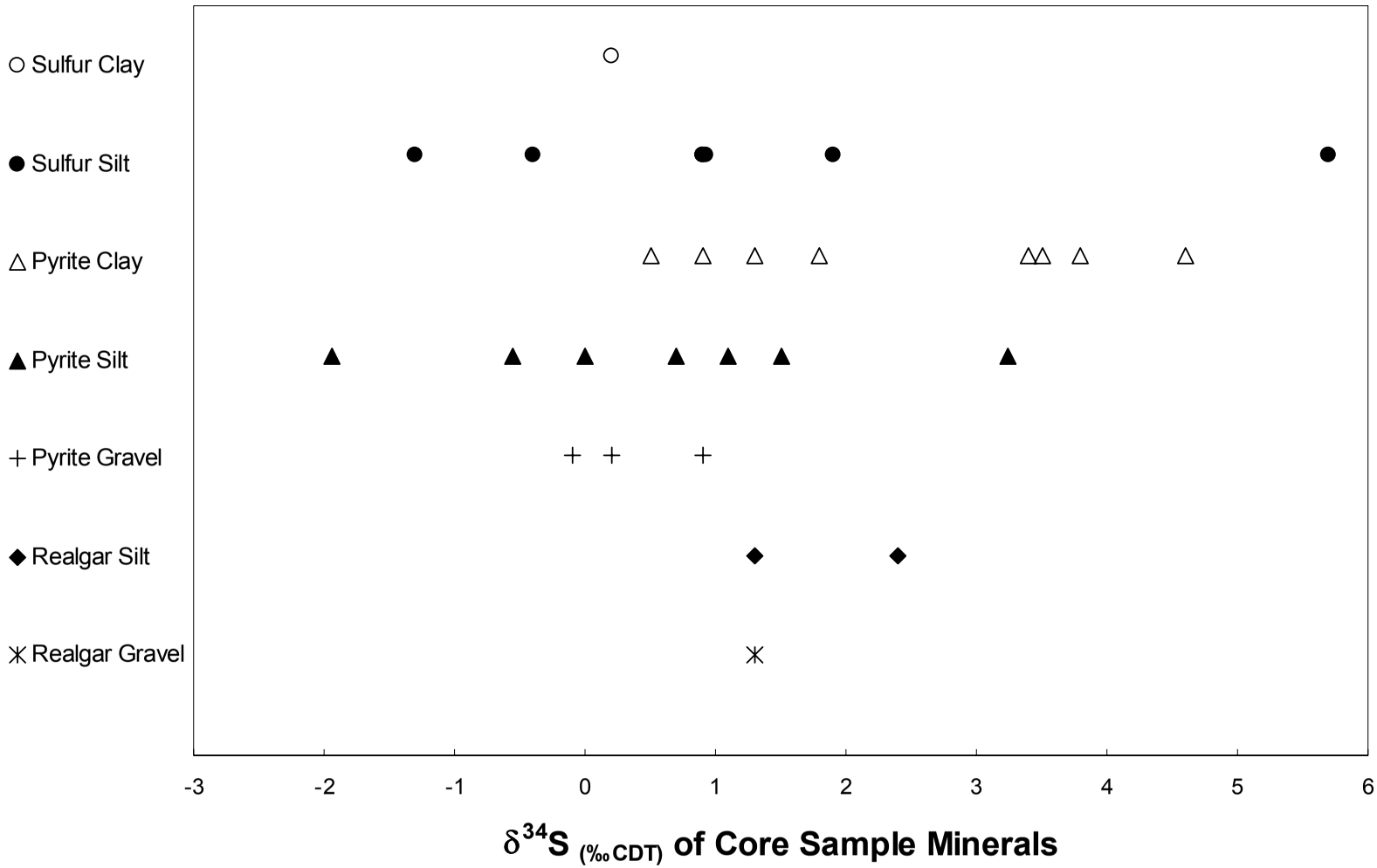
Sulfur Clay
Sulfur Silt
Pyrite Clay
Pyrite Silt
Pyrite Gravel
Realgar Silt
Realgar Gravel
-3
-2
-1
0
1
2
3
4
5
6
δ34S (‰CDT) of Core Sample Minerals

Fig. 10. $\delta^{34}S$ values of minerals from various core samples in relation to the depth at which they were separated from the core.

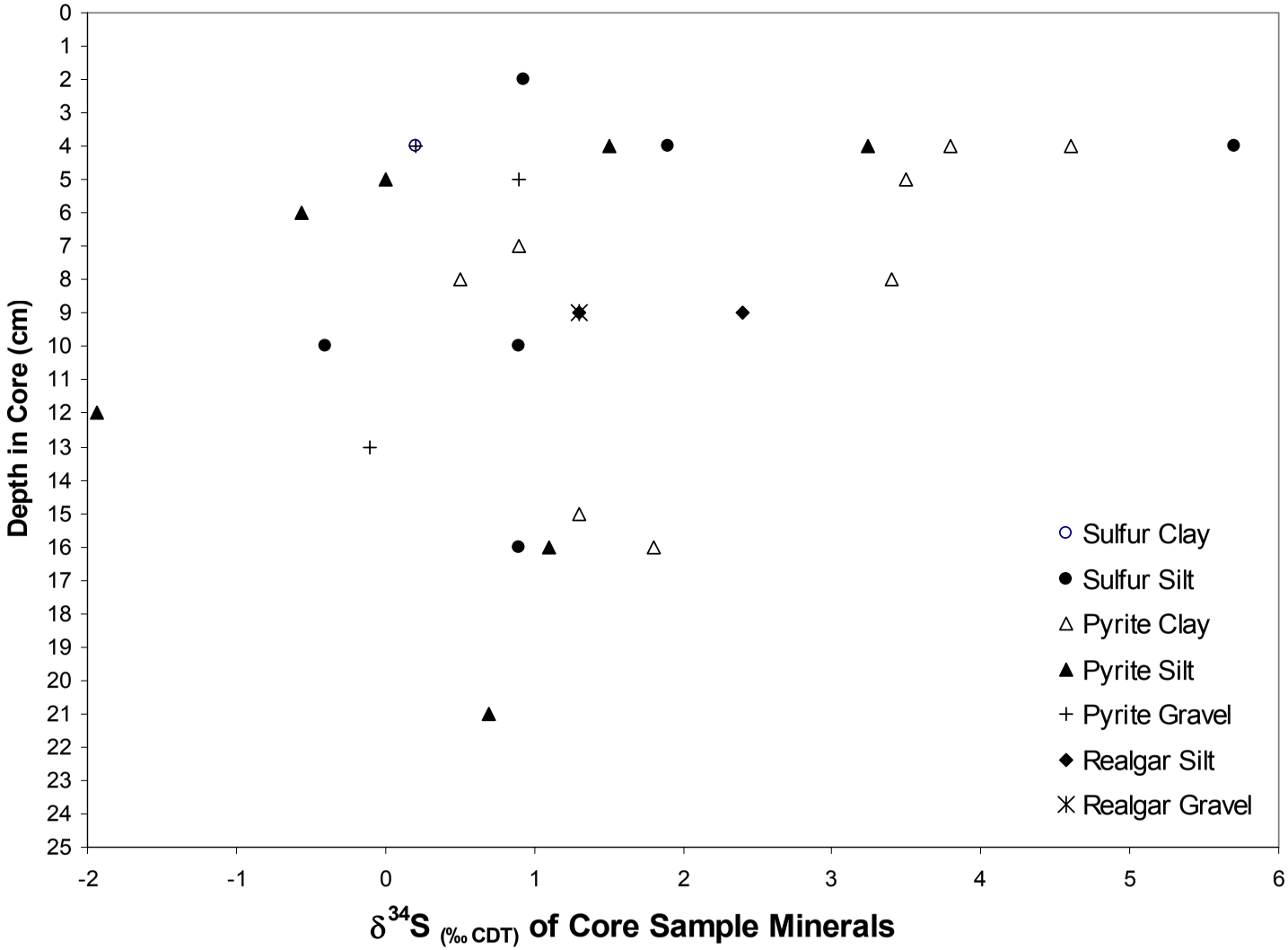
Depth in Core (cm)
0
1
2
3
4
5
6
7
8
9
10
11
12
13
14
15
16
17
18
19
20
21
22
23
24
25
-2
-1
0
1
2
3
4
5
6
δ34S (‰ CDT) of Core Sample Minerals
Sulfur Clay
Sulfur Silt
Pyrite Clay
Pyrite Silt
Pyrite Gravel
Realgar Silt
Realgar Gravel

CHAPTER 4: DISCUSSION

4.1 Water Chemical and $\delta D/\delta^{18}O$ Isotope Geochemistry

Acid-Sulfate Waters

It is interesting to note that pools containing the acid-sulfate waters appear to be the pools with signatures that fall closest to the field defined for magmatic waters (Primary Magmatic Water box) as measured by δD /$\delta^{18}O$ isotopic data. A discrepancy arises though, when looking at the accompanying chemical data. Concentrations of elements considered to be associated with magmatically derived waters, such as Cl, Li, and B, are lacking in these samples.

Craig et al. (1963) found that both O and H isotopes could be modified from their initial values during evaporative processes via kinetic isotope effects. When applied to higher temperature geothermal environments, the expression of this effect is consistent with the linear enrichment trends (slopes between 2 and 3, maximum 3.8 if boiling) observed for thermal waters plotted on δD vs. $\delta^{18}O$ diagrams (Giggenbach, 1978; Sheppard and Lyon, 1984; Varekamp and Kreulen, 2000). A distinguishing feature of acid-sulfate waters on these δD vs. $\delta^{18}O$ diagrams is their tendency to plot along lines that originate directly from a point along the local MWL as opposed to branching off from a point along a preexisting mixing trend (Criss and Taylor, 1986). This can be seen in a plot of δD vs. $\delta^{18}O$ for the acid sulfate waters of Uzon (Fig. 11).

Other studies of acid-sulfate systems show that evaporative enrichment is typically driven by heat supplied via the continual injection of steam released from a boiling horizon at depth (White et al., 1971). Not only does this mechanism produce the linear trend in the acid-sulfate δD vs. $\delta^{18}O$ plot, but it also provides a means for explaining various aspects of the pool chemistry. If a boiling horizon were present, it would effectively prevent the migration of nonvolatiles (i.e. Cl^-) and simultaneously partition H_2S into the vapor fraction. The H_2S could then redissolve in a perched aquifer at the surface, oxidize, and form the SO_4^{-2} characteristic of this type of water (Hedenquist, 1991; Marini et. al., 2002). Additionally, the acidity generated would promote enough host rock dissolution to elevate

Fig. 11. δD vs. $\delta^{18}O$ values for acid sulfate and meteoric water samples collected from the Uzon Caldera. Dashed line has a slope of 2.67 indicating boiling evaporative processes as the cause of isotopic enrichment.

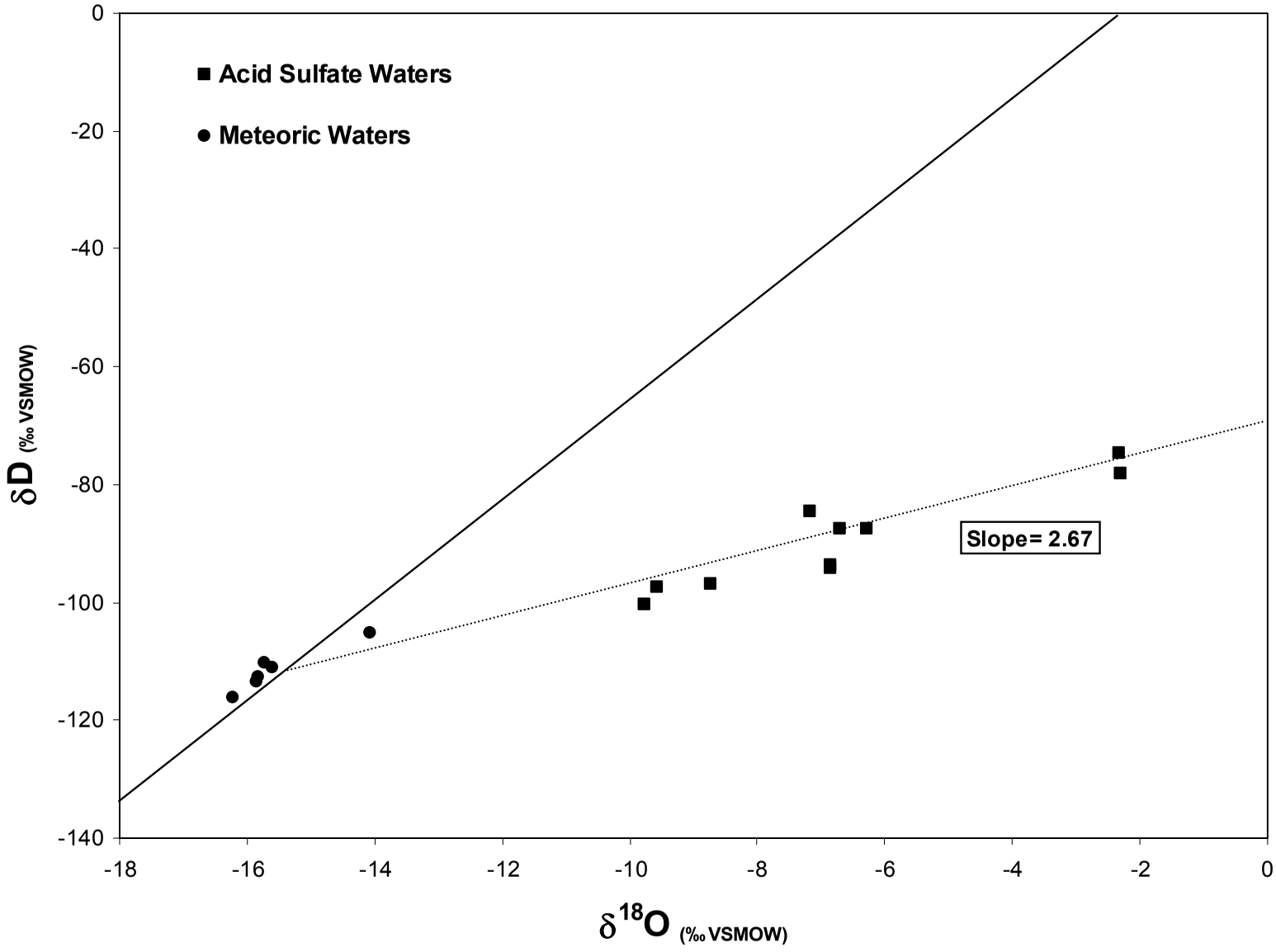
Acid Sulfate Waters
Meteoric Waters
Slope= 2.67
δD (‰ VSMOW)
δ18O (‰ VSMOW)
0
-20
-40
-60
-80
-100
-120
-140
-18
-16
-14
-12
-10
-8
-6
-4
-2
0

Na, K, Ca, and Mg concentrations to levels closely approaching that of the rock (Hedenquist, 1991). The acid-sulfate waters in Uzon display all these features. The elevated As and Sb values found in the acid-sulfate pools of the WTF reflect either rock dissolution and/or a form of vapor complexation and transport that produces the observed values (Giggenbach and Goguel, 1989).

Alkali-Chloride Waters

Given that the relatively high δD and $\delta^{18}O$ values characteristic of acid-sulfate waters are due to high evaporation rates, another mechanism is needed to explain the elevated δD and $\delta^{18}O$ values of the alkali-chloride waters. Although these waters, when plotted on a δD vs. $\delta^{18}O$ diagram, all lie along a line having a slope between 2 to 3 suggestive of evaporative enrichment (Fig. 12), chemical data show none of the signatures indicative of intensive steam-heating such as the high SO_4^{-2} concentrations, or a lack of non-volatile phases (ie. Cl^- and Li). Additionally, the similarity between the dissolved ion and isotopic chemistry of the thermal well sample[1], as well as its spatial proximity to the other alkali-chloride pools, implies a common process of formation for all waters. Because the well sample fluids are not formed by evaporative processes, the associated surface pools are similarly excluded from having their isotopic signature significantly altered via evaporative enrichment. Instead, the high elemental concentrations and enriched $\delta D/\delta^{18}O$ values for the alkali-chloride waters are the result of having primary magmatic fluids migrate towards the surface with subsequent dilution during mixing with deeply convecting meteoric waters.

Although it has been demonstrated that 1) the majority of elemental constituents present in thermal waters can be derived by the leaching of host rock by meteoric waters at high temperatures (Ellis and Mahon, 1967; Reyes and Vickridge, 1996) and 2) deeply convecting water of purely meteoric origin is the dominate component for most hydrothermal systems (especially those of

[1] The artificial pressure drop induced by the presence of the thermal well in the subsurface has subsequently generated a "wet steam" composed of both a vapor and an entrained alkali-chloride fluid phase. It is this entrained fluid phase that composes the majority of the 16m well sample as indicated by the presence of high concentrations of the non-volatile phases in the water chemistry.

Fig. 12. δD vs. $\delta^{18}O$ values for alkali chloride and meteoric water samples collected from the Uzon Caldera: Dashed line has a slope of 2.12, which is typically indicative of evaporative enrichment. However, in the case of alkali-chloride waters, this observed trend is due to fluid mixing between a local meteoric and a primary magmatic water endmember.

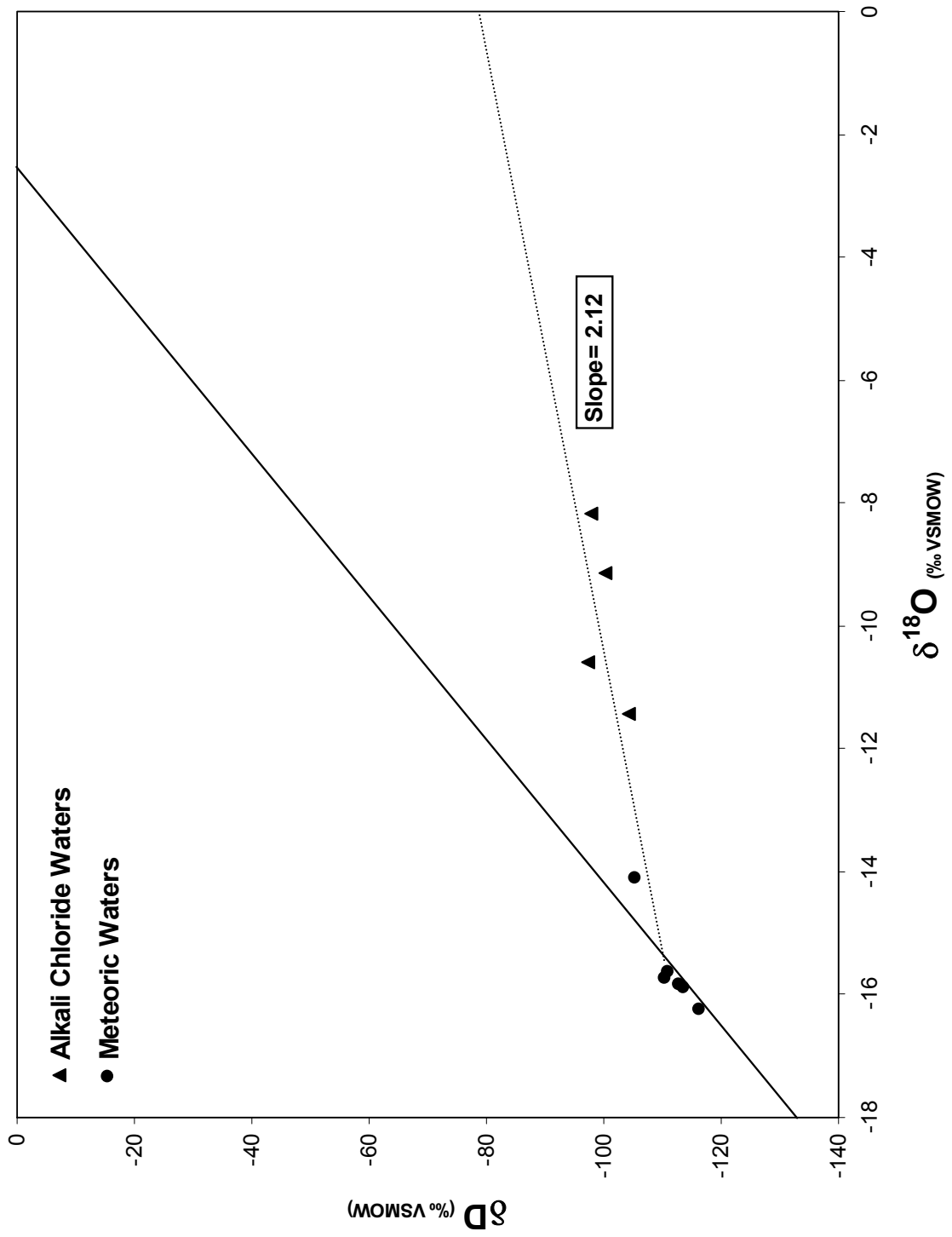
▲ Alkali Chloride Waters
● Meteoric Waters
Slope= 2.12
δD (‰ VSMOW)
δ18O (‰ VSMOW)
0
-20
-40
-60
-80
-100
-120
-140
-18
-16
-14
-12
-10
-8
-6
-4
-2
0

epithermal character) (Field and Fifarek, 1985), this alternative explanation of having deeply convecting meteoric waters leaching out the dissolved ion components at high temperatures to ultimately form alkali-chloride waters does not apply in the case of Uzon, in light of the δD and $\delta^{18}O$ data. The alkali-chloride waters of Uzon show no sign of being oxygen isotope shifted, as described by Sheppard (1986), which would accompany such deep, high temperature (≥400°C) meteoric water-rock interaction needed for extensive leaching of elemental constituents such as Cl, Li, and B (Ellis and Mahon, 1967). This is readily demonstrated by comparing alkali-chloride waters from Uzon to other active systems on a δD vs. $\delta^{18}O$ diagram (Fig. 13). The positive correlation between $\delta^{18}O$-shifted waters and chloride enrichment via leaching is well documented (Field and Fifarek, 1985; Sheppard, 1986), and the lack thereof in Uzon's alkali-chloride waters indicates that the elemental components, as well as the isotopic signatures, can only be magmatic in origin. The proximity of a magma body beneath the caldera to the surface, as indicated by geophysical data, is consistent with this conclusion.

Several factors may contribute to the suppression of boiling that is necessary for a component of the magmatic fluids to be able to reach the surface. Initially, as hot magmatic fluids migrate upward, the decrease in pressure is balanced by decreasing temperature as they encounter and mix with deeply convecting meteoric water. This mixing and cooling can suppress boiling during a portion of the fluid's ascent, but eventually decreasing pressure is no longer balanced by a sufficient decrease in temperature. At this point, boiling beneath Uzon's vapor-dominated areas (such as the WTF) occurs. In low-lying areas (~600m) such as the CETF, EETF, and Lake Fumarol'Noye, where large amounts of meteoric waters collect, ascending fluids encounter a thick column of cold surface water to form a hydraulically interconnected reservoir. The hydrostatic pressure and cold dilution provided by the meteoric column may have a "quenching" affect thereby preventing boiling (Hedenquist, 1991). This, in combination with subsurface heterogeneities in permeability and pressure, allows for minor amounts of the ascending fluid from the high temperature reservoir to be discharged at the surface.

This addition of fluid from below is consistent with the general observation that alkali-chloride waters tend to have higher discharge rates than those of vapor fed acid-sulfate pools (White et al, 1971).

Dilute Mixtures and Cold Surface Meteoric Waters

Thermal waters with relatively low δD and $\delta^{18}O$ values are most likely the result of the mixing and dilution of the alkali-chloride type end member fluid with significant amounts of cold surface meteoric waters. A small amount of isotopic enrichment via evaporation is likely, and would not be inconsistent with the observed isotopic and elemental data, although it should be noted that the heating mechanism driving the evaporation, and thus the degree to which evaporation occurs, is different from that taking place in the acid sulfate type waters, as indicated by the lack of acidity and sulfate concentration.

A small group of mixed waters in which the highest input of alkali-chloride component was found (i.e. those pools with the highest concentration of the alkali-chloride associated elements) are easily identified by anomalously high Li values. In order to have retained the high concentrations of Li but not the other elements that are typically found in alkali-chloride waters, it is probable that during the fluid transport and mixing process, alteration mineralization that normally partitions Li out of the fluid phase (i.e. formation of quartz, chlorite, illite-smectite, or pyrite) did not occur in and around these pools (Reyes and Vickridge, 1996). In terms of their O and H isotopic characteristics, these high Li waters show isotopic enrichments comparable to the alkali-chloride end member, as opposed to the other, more dilute mixed waters, whose O and H isotope values always plot on the depleted end of the mixing trend.

4.2 Rock Mineral $\delta^{34}S$ Compositions

Fumarole Precipitates and Vapor Alteration Minerals

Any portion of H_2S gas that does not dissolve as an aqueous phase within the hydrothermal system will rapidly oxidize once it reaches the surface by reacting with atmospheric O_2 within unsaturated steam heated soils and fumaroles via reactions (1) and (2). This oxidation occurs at

Fig.13. A comparison between the δD and $\delta^{18}O$ values of alkali chloride waters in the Uzon Caldera and near neutral chloride-bearing geothermal waters of other systems. Note the dominance of thermal waters with meteoric origins as indicated by the ^{18}O shift resulting from meteoric water-rock interaction in nearly all systems (with the exception of the meteoric-seawater mixing seen in Reykjanes). Uzon shows a clear enrichment of both isotopes, consistent with mixing of meteoric and magmatic fluids (modified after Sheppard, 1986).

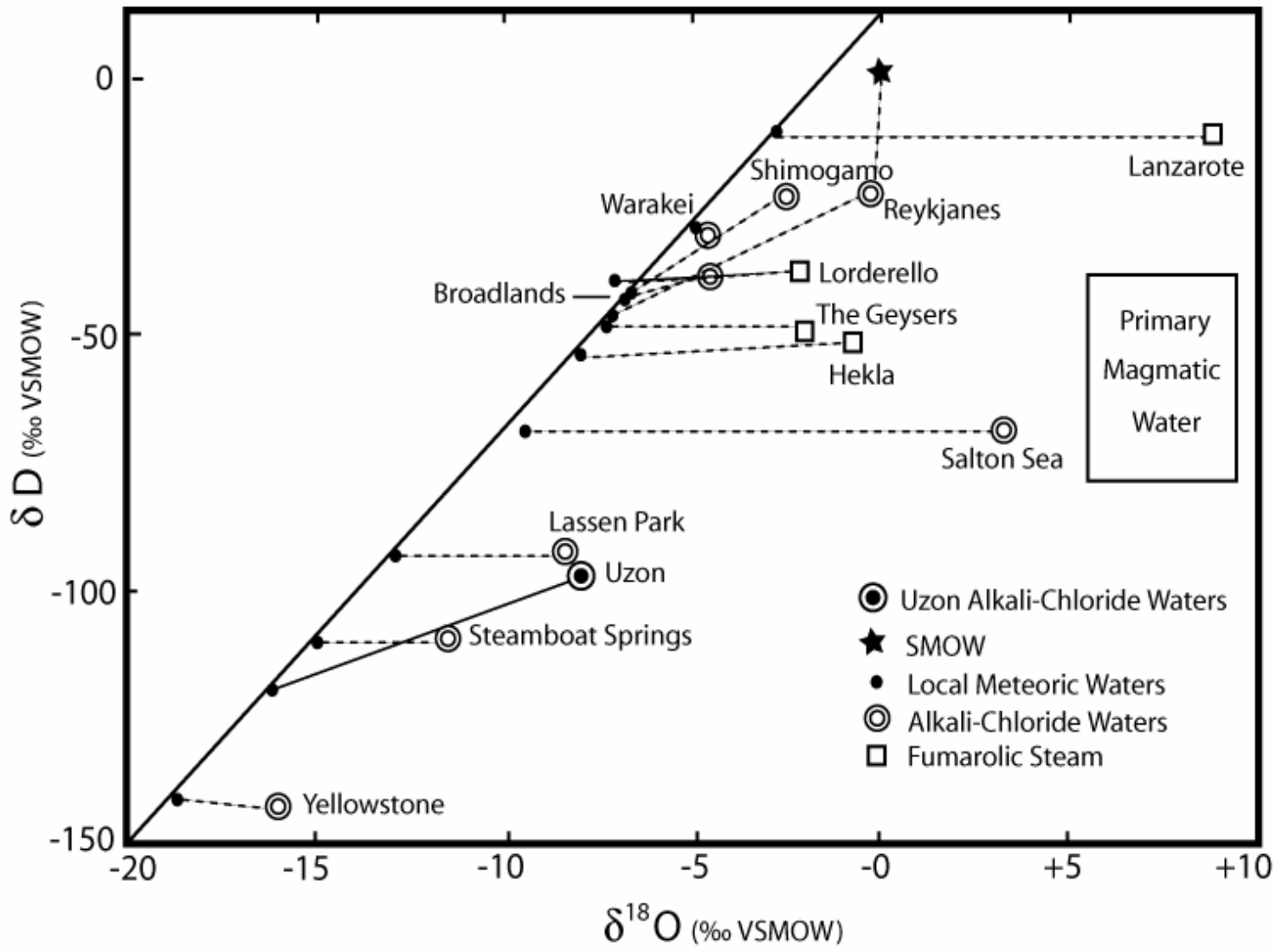
0
-50
-100
-150
δ D (‰ VSMOW)
-20
-15
-10
-5
-0
+5
+10
δ18O (‰ VSMOW)
Lanzarote
Shimogamo
Reykjanes
Warakei
Lorderello
Broadlands
The Geysers
Hekla
Salton Sea
Lassen Park
Uzon
Steamboat Springs
Yellowstone
Primary Magmatic Water
Uzon Alkali-Chloride Waters
SMOW
Local Meteoric Waters
Alkali-Chloride Waters
Fumarolic Steam

temperatures low enough for isotopic fractionation to be kinetically controlled (rather than equilibrium controlled), such that the overall rate of the reaction plays a part in the degree of fractionation between species (Ohmoto and Goldhaber, 1997). As shown in earlier studies, this abiotic oxidation of hydrogen sulfide to sulfur does not substantially change the ratio of sulfur isotopes between the species (Rafter et al., 1960). We therefore assume that the $\delta^{34}S$ values of the resulting minerals collected from Uzon from within and around fumaroles to represent the $\delta^{34}S$ of the parent H_2S gas. Such a tight clustering of $\delta^{34}S$ values for the minerals actively precipitating from fumaroles and vapor condensation between fields implies a common, homogenized $H_2S_{(g)}$ source currently beneath the caldera. Those minerals precipitated from H_2S gases exsolved earlier in the caldera's history show significantly lower values compared to modern equivalents. This likely reflects a progressive ^{34}S enrichment of the gas phase during the course of the hydrothermal system's evolution. Further investigation of the isotopic and chemical origin of the $H_2S_{(g)}$ currently emanating will be discussed in the next section.

4.3 Water $\delta^{34}S$ Sulfate Compositions

Acid-Sulfate Waters

The presence of acid-sulfate waters at the surface is indicative of a vapor-dominated environment below. The only magmatically derived sulfur species that can therefore reach the surface are either H_2S volatilized from a boiling horizon at depth or H_2S vapors exsolved directly from a magma. Taking the average $\delta^{34}S$ value calculated from the mineral analyses listed in Table 2 to represent the $\delta^{34}S$ value of the $H_2S_{(g)}$ in the vapor-dominated environment, $\delta^{34}S$ values of the gas should then closely approach ~+0.8‰.

As vapor streams through perched aquifers situated at the surface**,** a portion of the $H_2S_{(g)}$ will dissolve within an aqueous phase despite the especially low solubility of H_2S in low pH/high temperature conditions. Although no experiments have been conducted to determine if kinetic effects are expressed in S-isotope fractionation between $H_2S_{(g)}$-$H_2S_{(aq)}$, experimental results of equilibrium

fractionation by Szaran (1996) have shown a minor +1.1‰ enrichment in the aqueous phase at 30°C. Because kinetic fractionations are usually less than those occurring at equilibrium, negligible fractionation is expected during the condensation process (Ohmoto and Goldhaber, 1997).

According to the thermodynamics and kinetics of reactions involving $H_2S_{(aq)}$, the low pH of the acid-sulfate waters greatly restricts chemical reactions once the gas has dissolved in a liquid. Not only does low pH limit the aqueous sulfide speciation to the undissociated H_2S species, but it also kinetically inhibits dissolved O_2 from reacting with $H_2S_{(aq)}$ to form its various oxidized counterparts (i.e. S^0, SO_3^{-2}, $S_2O_3^{-2}$, SO_4^{-2}) (Millero, 1986). Zinder and Brock (1976) found that Fe^{+3}, which is prevalent in nearly all acid-sulfate pools, acts as the oxidizing agent instead, thus allowing $H_2S_{(aq)}$ oxidation to proceed rapidly via the reaction (Delmelle et al., 2000):

$$Fe^{+3} + H_2S \rightarrow S^0 + Fe^{+2} + 2H^+ \qquad (3)$$

Due to the kinetic control of fractionation at these temperatures, negligible isotopic partitioning takes place between the two sulfur species (Shoen and Rye, 1970). Although Fe^{+3} is a highly efficient oxidizer of H_2S at low pHs, the reaction proceeds only so far as S^0, and is therefore not capable of forming the significant quantities of H_2SO_4 characteristic of acid-sulfate pools. Instead, the H_2SO_4 is produced biogenically. Within the acidic conditions of these pools, the two most likely bacterial candidates for this reaction are *Thiobacillus thiooxidans* and *Sulfolobus acidocaldarius* (*T. thiooxidans* being prevalent between 30-55°C and *S. acidocaldarius* between 55-90°C)(Fliermans and Brock, 1972; Zinder and Brock, 1976). Not only does *S. acidocaldarius* oxidize S^0, but it also oxidizes Fe^{+2} (along with other bacteria such as *Thiobacillus ferrooxidans*), thus maintaining a steady supply of Fe^{+3} needed to continue abiotic oxidation of $H_2S_{(aq)}$ (Brock et al., 1975). Laboratory experiments show that biologic oxidation of S^0 to H_2SO_4 by these bacteria results in either no S isotope fractionation, or a slight ^{34}S enrichment of about +2‰ in the sulfate (Schoen and Rye, 1970). Assuming the $H_2S_{(g)}$ to be adequately represented by the $\delta^{34}S$ values of vapor mineral proxies shown in Table 2 (-1.5 to +1.6‰), the calculated $\delta^{34}S$ values for H_2SO_4 in Uzon's acid-sulfate waters should fall within the -1.5 to 3.6‰

range if we take into account the maximum possible fractionation the bacteria are capable of producing (+2‰). In looking at the observed $\delta^{34}S$ values for H_2SO_4 (-1.2 to +0.3‰), it appears that all values lie within this -1.5 to 3.6‰ calculated range.

Alkali-Chloride Waters

Because heat and mass of the alkali-chloride waters are transported via a liquid phase, the non-volatile components representing (in part) the deeper fluid are able to reach the surface. This includes deeply derived, non-volatile SO_4^{-2} formed during the disproportionation of magmatic SO_2 deep below the surface (Giggenbach, 1987). Despite the chemical and isotopic inertness of this "deep sulfate" at surface temperatures (Spirakis, 1984), its $\delta^{34}S$ isotopic signature can be altered once it discharges at the surface and undergoes mixing with the isotopically lighter bacterially generated sulfate as observed in the Orakeikorako thermal field in New Zealand (Sheppard and Lyon, 1984). $\delta^{34}S$ values in Table 1 show a large spread of values in the alkali-chloride pools, suggesting that variable amounts of mixing between this "deep sulfate" and the "surficial sulfate" has occurred. In order to determine the extent of contamination and possibly the source, it is necessary to calculate the original, non-contaminated $\delta^{34}S$ signature of the deep sulfate, using a hypothetical model of the Uzon hydrothermal system. This model evaluates bulk isotopic value ($\delta^{34}S_{\Sigma}$) of the magma source, and the subsequent processes fractionating the sulfur as it migrates towards the surface. Figure 14 summarizes the processes according to the environments in which fractionation takes place.

Fractionation Model

(0) <u>The Crystallizing Magma Source:</u> Recent investigations by Marini et al. (2002) and Hoog et al. (2001) show the $\delta^{34}S_{\Sigma S}$ of arc-type magmas to typically fall between +4‰ and +7‰. A $\delta^{34}S_{\Sigma S}$ of +5‰ will be assumed for Uzon's magma, which is the same value reported by Ueda and Sakai (1984) for magmas of the nearby Japanese island arc system. Because of the minor fractionation (0.5‰) among all sulfide species at the high temperatures found within crystallizing magmas (ie. H_2S, FeS liquid and crystals, Fe_3SO_2, and/or SH^-), removal of up to 95% of the original sulfur in the form of

Fig. 14. Schematic section through the Uzon Caldera summarizing the environments in which S isotope fractionating processes take place. Note the roles of topography and the subsequent vapor vs. liquid-dominated conditions in ultimately determining the S species and corresponding isotopic values that reach pools at the surface. Species shown with a star (*) are produced during disproportionation, and the associated isotopic values are calculated assuming equilibrium at 250ºC, the lowest temperature at which $SO_4^{-2}{}_{(aq)}$ can participate in chemical and isotopic reactions (Spirakis, 1984).

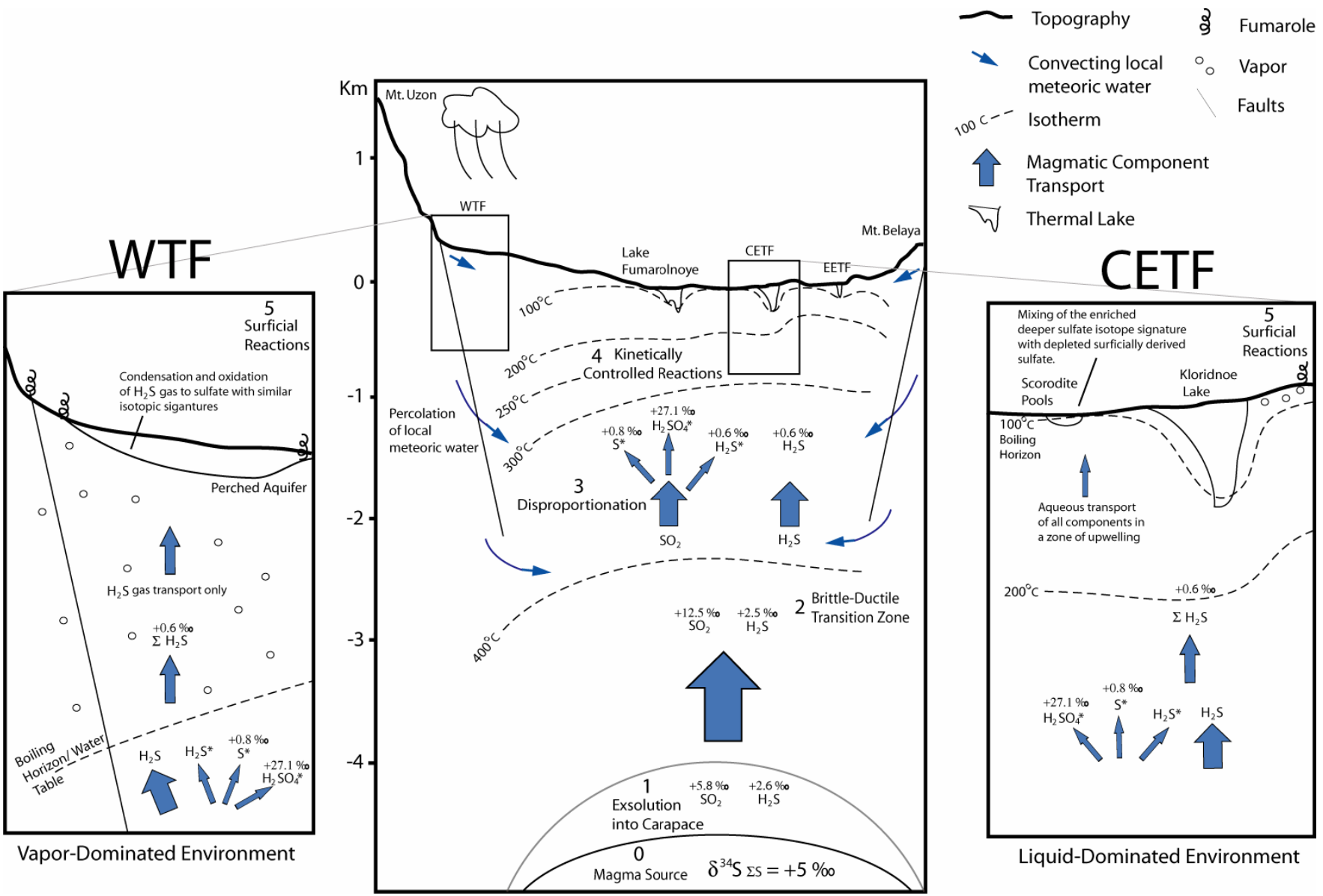
Topography
Convecting local meteoric water
Isotherm
Magmatic Component Transport
Thermal Lake
Fumarole
Vapor
Faults
WTF
CETF
Km
Mt. Uzon
WTF
Lake Fumarolnoye
CETF
EETF
Mt. Belaya
100°C
200°C
250°C
300°C
400°C
4 Kinetically Controlled Reactions
Percolation of local meteoric water
3 Disproportionation
+0.8 ‰ S*
+27.1 ‰ H2SO4*
+0.6 ‰ H2S*
+0.6 ‰ H2S
SO2
H2S
2 Brittle-Ductile Transition Zone
+12.5 ‰ SO2
+2.5 ‰ H2S
1 Exsolution into Carapace
+5.8 ‰ SO2
+2.6 ‰ H2S
0 Magma Source
δ34S ΣS = +5 ‰
5 Surficial Reactions
Condensation and oxidation of H2S gas to sulfate with similar isotopic sigantures
Perched Aquifer
H2S gas transport only
+0.6 ‰ Σ H2S
Boiling Horizon/ Water Table
H2S
H2S*
+0.8 ‰ S*
+27.1 ‰ H2SO4*
Vapor-Dominated Environment
Mixing of the enriched deeper sulfate isotope signature with depleted surficially derived sulfate.
Scorodite Pools
Kloridnoe Lake
100°C Boiling Horizon
Aqueous transport of all components in a zone of upwelling
200°C
+0.6 ‰ Σ H2S
+27.1 ‰ H2SO4*
+0.8 ‰ S*
H2S*
H2S
Liquid-Dominated Environment

crystals such as pyrrhotite from the melt would result in less than ±1.5‰ fractionation between the newly formed mineral species and the remaining melt via Rayleigh fractionation (Ohmoto and Goldhaber, 1997). Because this fractional crystallization has such a minor S isotopic effect on the magma's subsequent S isotopic signature, our model will assume the initial $\delta^{34}S$ value of the magma (+5‰) to also represent the $\delta^{34}S$ of the sulfur species subsequently exsolved during the magma's cooling (ie. SO_2 and H_2S).

(1) Exsolution From Magma- Sulfur is exsolved into a fluid-rich carapace during crystallization of the magma. While fluids remain in this carapace, chemical and isotopic equilibrium is maintained with the magma (Rye, 1993). Redox conditions continue to be governed by the f_{O2} of the magma, and, in the case of shallowly emplaced I-type magmas such as Uzon, f_{O2} is assumed to be moderately high (Giggenbach, 1997). With such oxidizing conditions, the speciation of the exsolved sulfur includes SO_2 in addition to H_2S. Because of the shallow nature of the magma below Uzon, the ratio between the two species being exsolved (H_2S/SO_2) is expected to be < 1 due to the lower P_{H2O} (Ohmoto and Goldhaber, 1997). For our model, an H_2S/SO_2 ratio of 1:3 and a temperature of 850°C will be assumed. The following equations are used to calculate the resulting $\delta^{34}S$ values of the exsolved species:

$$\delta^{34}S_{H2S} = \delta^{34}S_{\sum S} - \Delta_{H2S\text{-}SO2}\,(X_{SO2}/100) \qquad (4)$$

$$\delta^{34}S_{SO2} = \delta^{34}S_{\sum S} + \Delta_{H2S\text{-}SO2}\,(X_{H2S}/100) \qquad (5)$$

where $\delta^{34}S_{\sum S}$ is the bulk sulfur isotopic ratio of the system (+5‰), $\Delta_{H2S\text{-}SO2}$ is the equilibrium fractionation at the assumed temperature (3.2‰ at 850°C) (Ohmoto and Rye, 1979), and x_{H2S} and x_{SO2} are the molar percents of the species involved (25 and 75% respectively). Using the above values, the calculated $\delta^{34}S$ values of H_2S and SO_2 in this environment are +2.6 and +5.8‰, respectively.

(2) The Brittle-Ductile transition zone: When SO_2 and H_2S move through the carapace and enter the brittle-ductile transition zone (Rye, 1993), significant changes occur in the redox state of the fluids due to the buffering capacity of iron bearing minerals present within the country rock. As opposed to the preference of the fluids themselves to internally buffer redox species towards more oxidized conditions with decreasing pressure, the di-trivalent iron redox pair within the rock act to reduce the SO_2 to H_2S via the following reaction (Giggenbach, 1987):

$$SO_2 + 6(FeO) + H_2O \leftrightarrow H_2S + 6(FeO_{1.5}) \quad (6)$$

For this stage of the model, the new H_2S/ SO_2 ratio is assumed to be 3:1. At 400°C (the approximate temperature the for brittle ductile transition (Rye, 1993), the equilibrium $\Delta_{SO2\text{-}H2S} = +9.8‰$ (Ohmoto and Goldhaber, 1997). So given $X_{H2S} = 75\%$ and $X_{SO2} = 25\%$, the calculated $\delta^{34}S$ values of the H_2S and SO_2 are +2.5 and +12.4‰, respectively.

(3) < 400°C Disproportionation: As fluid temperatures decrease from 400°C to roughly 250°C, SO_2 becomes unstable and begins to disproportionate according to the following two reactions:

$$4SO_2 + 4H_2O \leftrightarrow 3H_2SO_4 + H_2S \quad (7)$$

$$3SO_2 + 3H_2O \leftrightarrow 2H_2SO_4 + S^0 \quad (8)$$

where (7) is the dominant reaction under higher temperature (400 to 350°C)/lower redox potential conditions and (8) is the dominant reaction under lower temperature (350 to 250°C)/higher redox potential conditions (Africano and Bernard, 2000; Kusakabe et al., 2000). The presence of isotopically enriched sulfate in alkali-chloride pools of other hydrothermal systems has been taken to be indicative of reaction (7) by previous workers (Sheppard and Lyon, 1984), while the presence of liquid elemental sulfur layers beneath several crater lakes (Lake Bannoe of Uzon being included in the study) suggest that reaction (8) can also take place (Kuskabe et al., 2000). The presence of both isotopically enriched sulfates and liquid elemental sulfur layers in Uzon, suggests that both reactions (7) and (8) occur beneath the surface. Taking all S species into account in the lower temperature

range (~250°C), Kuskabe et al. (2000) arranged the following equation to calculate the resulting $\delta^{34}S_{H2SO4}$ generated from the disproportionation:

$$\delta^{34}S_{H2SO4} = \delta^{34}S_{\sum S} + \Delta_{H2S}\, r/(1+r) + \Delta_S\, (1/3)\, 1/(1+r) \qquad (9)$$

where $\delta^{34}S_{\sum S}$ again represents the bulk sulfur isotopic ratio of the system, Δ_{H2S} and Δ_S represent the equilibrium fractionation factors for H_2SO_4-H_2S and H_2SO_4-S^0 respectively, and r equals the $\underline{H_2S/SO_2}$ ratio of the redox pair prior to disproportionation. Assuming equilibrium temperatures fall within the 250 - 275°C range (the lowest temperatures at which $SO_4^{-2}{}_{(aq)}$ can participate in chemical and isotopic reactions)(Spirakis, 1984), Δ_{H2S} and Δ_S values range from +26.5 to +24.3‰ (Sakai, 1968) and +26.3 to +24.3‰ (Kuskabe et al., 2000), respectively. If $\delta^{34}S_{\sum S}$ equals +5‰ and r = 3, the calculated uncontaminated $\delta^{34}S_{H2SO4}$ values will fall between +27.1 and +25.3‰. In order to validate the assumptions regarding temperature and H_2S/SO_2 made in equation (9), calculation of the accompanying $\delta^{34}S_{H2S}$ values produced during disproportionation should yield values ranging between +0.6 to +0.9‰. When compared to the average value of the observed $H_2S_{(g)}$ values obtained using the mineral proxies listed in Table 2 (+0.8‰), it appears that the assumptions made for the model are valid.

(4) $\underline{< 250°C \text{ Kinetically Based Reactions}}$: As the fluids cool to temperatures below 250°C, sulfur isotope exchange among most aqueous fluid sulfur species, as well as S-bearing mineral phases becomes extremely slow and is controlled by kinetic rather than equilibrium reactions (Kyser, 1987). Redox chemistry as well shifts from being equilibrium based to being kinetically based. This is especially important for SO_4^{-2}, which becomes kinetically inhibited from participating in any redox reactions. Not only does SO_4^{-2} become inert, but any additional sulfate formation via $H_2S_{(aq)}$ oxidation within the fluids also ceases. Thus, the isotopic signature of the deeply derived SO_4^{-2} (+27.1 to +25.3‰) is preserved as it migrates to the surface (Spirakis, 1984). A detailed investigation of the

water saturated sediments of the CETF by Migdisov et al. (1992) confirms the inert nature of sulfate by documenting chemical disequilibrium with all other aqueous and solid sulfur species present. Despite such isotopic and chemical stability, preservation of the deep sulfate's isotopic signature once it has reached the surface is prevented by an influx of significant amounts of SO_4^{-2} formed via surficial processes. The distribution of relatively low $\delta^{34}S_{H2SO4}$ (+13.2 to +7.6‰) compared to the calculated $\delta^{34}S_{H2SO4}$ values for deep seated SO_4^{-2} (+27.1 to +25.3‰) implies that these surficial processes are the result of the series of abiotic and biotic $H_2S_{(g)}$ oxidation reactions.

(5) Surficial Reactions: The low pH values of the alkali-chloride pools (much like the acid-sulfate waters) allows $H_2S_{(aq)}$ oxidation only in the presence of Fe^{+3} rather than O_2 (Zinder and Brock, 1976)(Millero, 1986). Iron concentrations in alkali-chloride waters are up to 3 orders of magnitude less than those found in acid sulfate pools, thus $H_2S_{(aq)}$ oxidation to S^0 is unlikely. Similarly, oxidizing activity by *S. acidocaldarius* is inhibited due to the increased salinity (> 1% NaCl) of the high temperature alkali-chloride waters compared to acid-sulfate waters (Brock et al., 1976). While *T. thiooxidans* may still be able to function at such high salinities, pool temperatures typically exceed the bacteria's maximum survivable temperature of 55°C. Elemental, pH, and temperature conditions for the water-saturated substrate surrounding these pools, as measured in a study by Cleverley et al. (2003), are similarly noncondusive to chemical and bacterial generation of SO_4^{-2}.

As discussed previously, water precipitated either as rain or snow within the caldera percolates and flows down from the higher elevation areas to ultimately collect in the marshy, lower elevations of the CETF, EETF, and Lake Fumarol'Noye. Although no abiotic/biotic oxidation of H_2S is likely immediately within and around the alkali-chloride pools in these lower elevation fields, SO_4^{-2} formed via the biochemical reactions within the soils of the higher elevation areas can be transported to the lower areas as runoff. Research by Mosser et al. (1973) found that the same *S. acidocaldarius* found in acid-sulfate pools is also capable of rapidly oxidizing large amounts of S^0 in soils. The close proximity of isolated acid-sulfate vapor features such as mud volcanoes, mudpots, and sulfidized soils

(referred to as sulfur hillocks by Karpov, 1998; see also erh-041 in Table 2) to the fields containing alkali-chloride pools, provides a conducive environment for either of the two sulfur oxidizing species (*S. acidocaldarius* and *T. thiooxidans*) to generate the $\delta^{34}S$ depleted sulfate.

Dilute Mixtures and Cold Surface Waters

The mixed waters, as expected, have $\delta^{34}S_{H2SO4}$ signatures falling closer to the bacterially produced SO_4^{-2} values (~0‰) than to those values observed in alkali-chloride pools (~+13.2 to +7.6‰) in most cases. This is due to the relatively small contribution of "deep sulfate" into these pools originating from the alkali-chloride zone of fluid upwelling beneath the CETF and Lake Fumarol'Noye. This causes the isotopic signatures of the dilute pools to be controlled by the influx of depleted (~0‰), biologically derived sulfate. Figure 15 shows the increase in surficial sulfate contribution to pool $\delta^{34}S_{H2SO4}$ signatures as distance increases from the zone of deep fluid upwelling for the CETF. Note that the high topography on the north side of the field is where localized vapor dominated conditions, also referred to as parasitic vapor zones (Allis, 2000), are producing the environment needed for bacterial generation of the depleted (~0‰) $\delta^{34}S_{H2SO4}$ reservoir.

In the EETF the $\delta^{34}S_{H2SO4}$ values of Lake Bannoe and Zavarsin Pool (+13.5 and +8.0‰ respectively) indicate some degree of deep plume upwelling from below, despite not having the dissolved ion concentrations indicative of the alkali-chloride type waters. Subsurface lateral flow of the deeply derived, ^{34}S-enriched SO_4^{-2} from the Lake Bannoe and Zavarsin Pool areas into the surrounding pools dominated by the depleted surficial sulfate would thus account for the sulfur isotopic values present in EETF (Fig. 16).

Fig. 15. Simplified map of the hydrothermal features of the CETF. Location of water sample sites with aqueous sulfate $\delta^{34}S$ values show a zone of enrichment indicating upwelling of deeply derived fluids along the center of the field. Relatively low values occur in the acid-sulfate waters perched in elevated ground to the north (modified from Karpov, 2005).

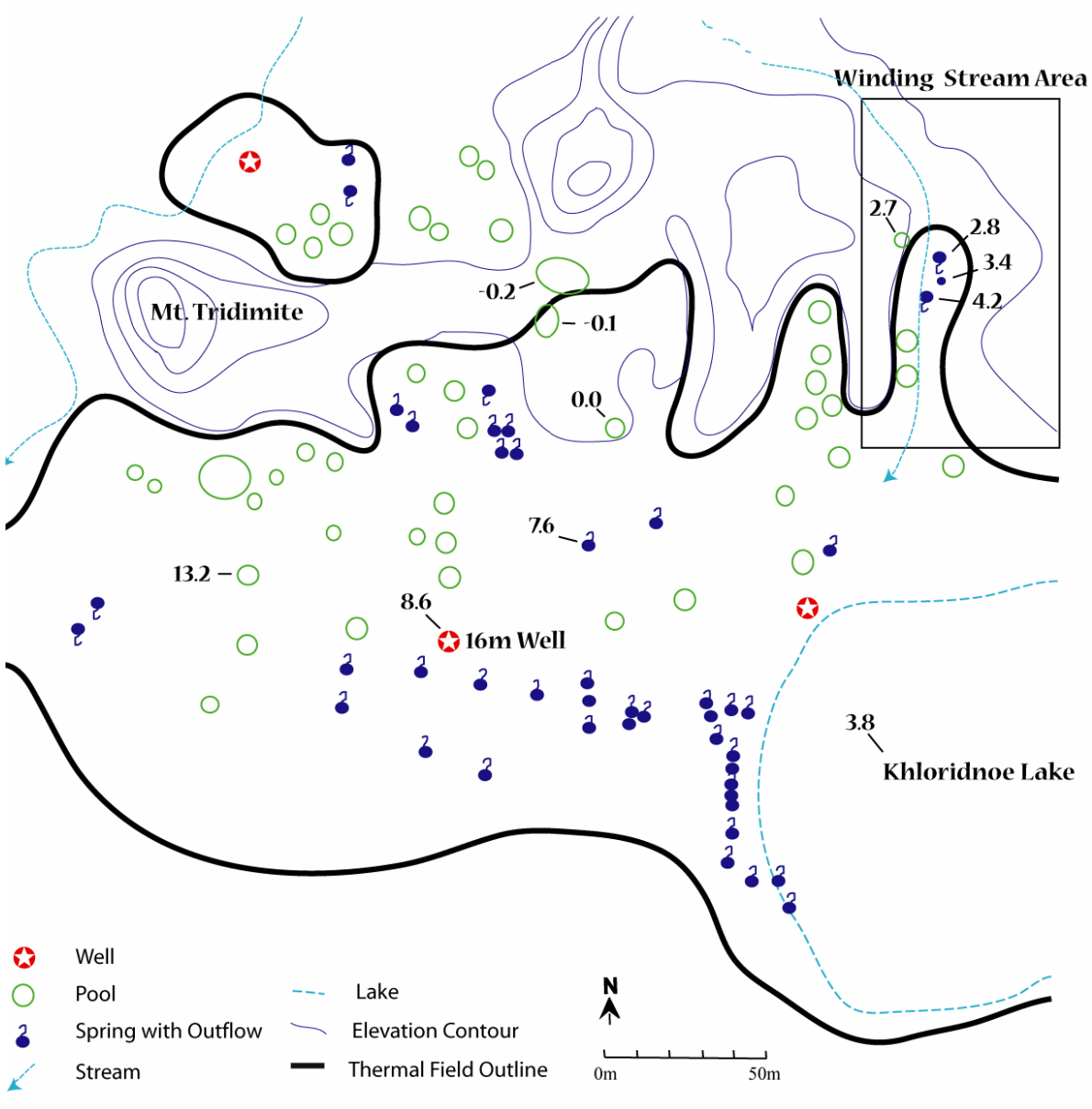
Winding Stream Area
2.7
2.8
3.4
4.2
Mt. Tridimite
-0.2
-0.1
0.0
7.6
13.2
8.6
16m Well
3.8
Khloridnoe Lake
Well
Pool
Spring with Outflow
Stream
Lake
Elevation Contour
Thermal Field Outline
N
0m
50m

Fig. 16. Simplified map of the hydrothermal features of the EETF. Location of water sample sites with associated aqueous sulfate $\delta^{34}S$ values show enrichment in Lake Bannoe and Zavarzin Pool indicating possible upwelling zones of deeply derived fluid beneath these areas (modified from Karpov, 2005).

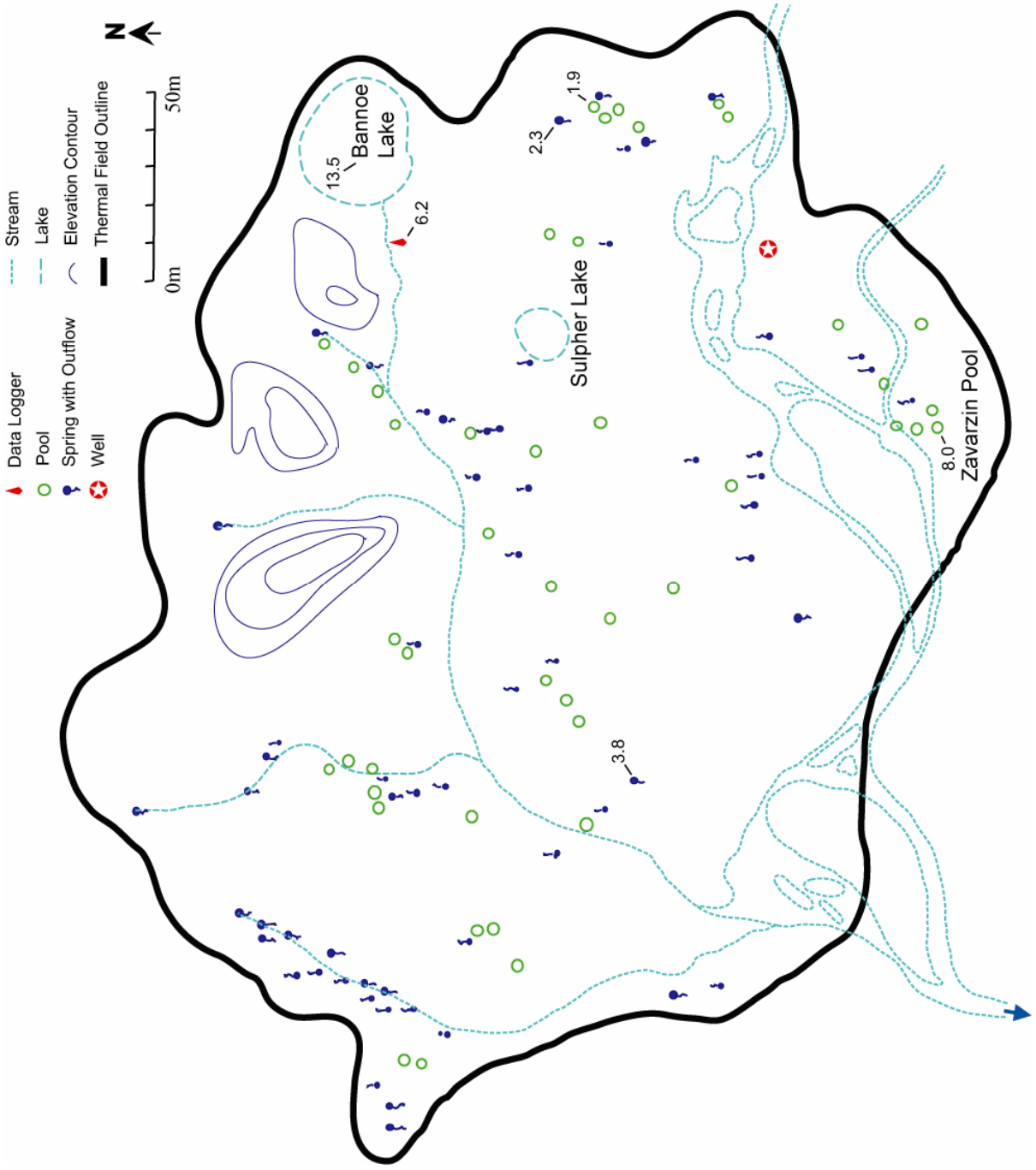
Stream
Lake
Elevation Contour
Thermal Field Outline
Data Logger
Pool
Spring with Outflow
Well
0m
50m
N
Bannoe Lake
Sulpher Lake
Zavarzin Pool
13.5
6.2
2.3
1.9
3.8
8.0

4.4 Core Sample Mineral $\delta^{34}S$ Compositions

Sediment Cores Samples from Vapor-Dominated Thermal Fields

Cores taken from in and around acid-sulfate pools show pyrite $\delta^{34}S$ signatures (+0.5 to +0.9‰) that are nearly identical to the values inferred for the $H_2S_{(g)}$ (-1.5 to +1.6 ‰) as well as the $\delta^{34}S$ values observed for the aqueous SO_4^{-2} extracted from the waters (-1.2 to 0.3‰)(Fig. 17). Because the only input of S into these areas is H_2S vapor, it is assumed that the pyrite is formed by kinetically controlled, nonfractionating reactions directly involving the dissolved $H_2S_{(aq)}$, and/or the reduction of the other aqueous components subsequently formed via abiotic and biotic reactions involving this $H_2S_{(aq)}$ (S^0 and H_2SO_4). Although there are thermophillic bacteria capable of reducing aqueous SO_4^{-2} to pyrite, the reaction is slow and results in kinetic fractionations anywhere between -15 and -60‰, and thus does not appear to be a viable step in the pyrite forming process (Ohmoto and Goldhaber, 1997). Abiotic sulfate reduction as well is not kinetically possible at such low temperatures (Spirakis, 1984). Instead, it is likely that pyrite formation in the vapor-dominated zones is limited to abiotic reactions involving either $H_2S_{(aq)}$ or S^0.

Overall, the limited variability seen in the sulfur isotope compositions of the various S-bearing phases found in vapor-dominated areas shown in Figure 17 is controlled by two factors. First, there is only one source ($H_2S_{(g)}$) of S for pools formed in vapor-dominated conditions. Second, the low pH inherent in these acid-sulfate pools constrains the number of possible reactions involved in transforming $H_2S_{(g)}$ into aqueous and mineral components (Millero, 1986).

Sediment Cores Samples from Liquid-Dominated Thermal Fields

As opposed to the tightly clustered $\delta^{34}S$ values found in the vapor-dominated environments, minerals taken within and around alkali-chloride and the dilute mixed pools show a wide range of $\delta^{34}S$ values both within core samples, and between sample locations (-1.9 to +5.7‰). This range partially overlaps the values determined for the $H_2S_{(g)}$ reservoir (-1.5 to +1.6 ‰), as well as the range observed for the alkali-chloride and dilute mixed waters' aqueous SO_4^{-2} (+1.9 to +13.5‰)(Fig. 17). The wider

Fig. 17. $\delta^{34}S$ values of the various S-bearing species collected from vapor vs. liquid-dominated environments. Included are values of the inferred $H_2S_{(g)}$ reservoir approximated using the fumarole precipitate and vapor alteration minerals of Table 2, the minerals extracted from core samples listed in Table 3, and the aqueous sulfate precipitated from the different thermal water types listed in Table 1. The values associated with the liquid-dominated areas show greater variability in their S-isotopes (for both mineral and aqueous phases) than do the values associated with the vapor-dominated areas.

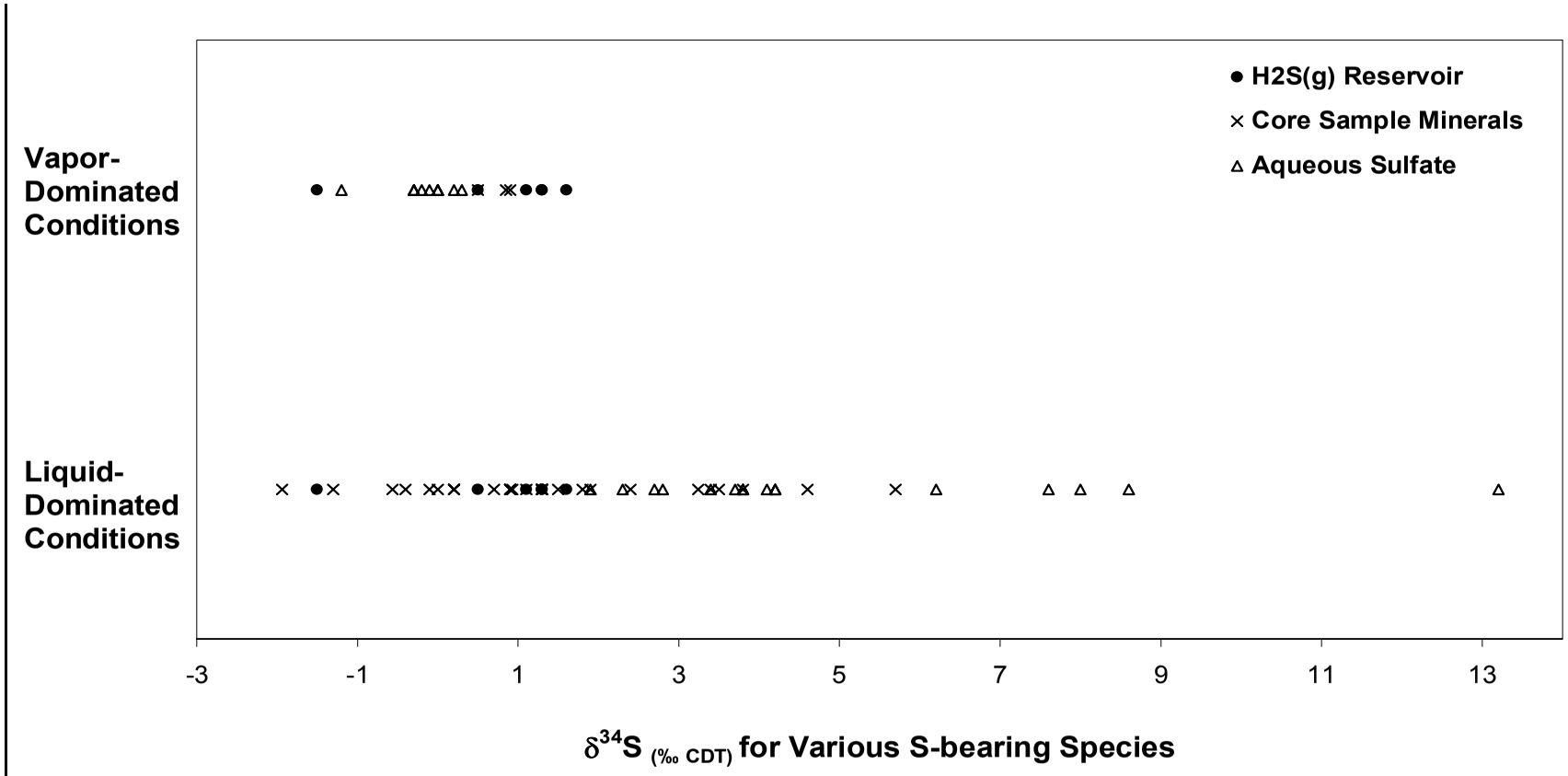
● H2S(g) Reservoir
× Core Sample Minerals
△ Aqueous Sulfate
Vapor-Dominated Conditions
Liquid-Dominated Conditions
-3
-1
1
3
5
7
9
11
13
δ34S (‰ CDT) for Various S-bearing Species

variability seen in the mineral $\delta^{34}S$ values produced is again, much like the vapor-dominated areas, likely tied to the source of S and the pH conditions of the pools. Within the liquid-dominated areas, there are a greater number of S bearing components accompanying the deeply derived fluids upwelling from below. This would include H_2S, "deep sulfate", ± any other nonvolatile S-bearing species capable of being transported in the liquid phase. The H_2S and deep sulfate have widely different isotope signatures that can influence the degree of enrichment or depletion in any minerals being precipitated abiotically or biotically using these two species as a S-source. Another potential factor in determining the variability is the higher pH found in the alkali-chloride and dilute mixed waters, which may allow a greater array of aqueous sulfur species to exist, as seen in the case of the various forms of reduced sulfur (ie. at pH= 6 speciation can include H_2S, HS^-, HS_4^-, S_5^{2-})(Millero, 1986). In order to accurately determine the reactions taking place to form the $\delta^{34}S$ values of the minerals from the liquid-dominated environments, a more detailed correlation between the chemistry for each pool and the minerals being precipitated is necessary. This is beyond the scope of this research.

CHAPTER 5: CONCLUSIONS

1) Examination of pH, isotope, and major element chemistry of thermal and non-thermal waters within Uzon Caldera shows four distinct water types: an acid-sulfate type (WTF and OTF), an alkali-chloride type (CETF and Lake Fumarol'Noye), a dilute mixing of the alkali-chloride fluids with non-thermal meteoric waters (CETF and EETF), and cold meteoric surface waters resulting from seasonal precipitation and melting (streams and Lake Dal'nee).

2) The $\delta^{34}S$ compositions of minerals actively precipitating from fumaroles and vapor condensation indicate a relatively homogenous $H_2S_{(g)}$ reservoir for the hydrothermal system. Comparison of the $\delta^{34}S$ values for minerals actively precipitating vs. minerals precipitated earlier in the caldera's history imply that the composition of the $H_2S_{(g)}$ reservoir has evolved with time.

3) The δD, $\delta^{18}O$, and $\delta^{34}S$ isotope data in conjunction with the elemental data indicate two different geologic/hydrologic environments responsible for forming the different fluid types: a vapor-dominated environment and a liquid-dominated environment. The physical and chemical processes associated with each environment result in specific pH, elemental, and $\delta D/\delta^{18}O/\delta^{34}S$ signatures for the resulting pools, springs, and mudpots. Although these processes are initially dictated by abiotic factors at depth, microbial influences play a major part in pool chemistry at the surface.

4) Sulfur isotope analysis of a variety of minerals extracted from core samples taken from both vapor and liquid-dominated environments show how important the conditions of pool formation are in determining the amount of mineral $\delta^{34}S$ variability. In vapor-dominated fields where there is only one source of sulfur ($H_2S_{(g)}$) and very few processes transforming it into aqueous and/or mineral species, there is limited variation in sulfur isotope composition. In liquid-dominated fields where there are several sulfur sources available and therefore a greater number of mineral forming processes potentially taking place, there is greater variation in the observed sulfur isotopic compositions both between and within individual mineral species.

REFERENCES

Africano, F., Bernard, A., 2000. Acid alteration in the fumarolic environment of Usu volcano, Hokkaido, Japan. J. Volcanol. Geotherm. Res. 97, 475-495.

Allis, Rick, 2000. Insights on the formation of vapor-dominated geothermal systems. Proc. World Geothermal Congress, May 28-June 10, Kyushu-Tohoku Japan, 2489-2496.

Belousov, V.I., Grib, E.N., Leonov, V.L., 1984. The geological setting of the hydrothermal systems in the Geysers Valley and Uzon Caldera. J. Volc. Seis., 5, 67-81.

Braitseva, O.A., Bogoyavlenskaya, G.E., and Erlikh, E.N., 1974. Geologic structure of the Uzon-Geizernaya Depression. In: S.I. Naboko (ed.), Volcanism, Hydrothermal Process and Ore Formation. Nedra, Moscow, 10-32. (in Russian)

Brock, T.D., Cook, S., Petersen, S., Mosser, J.L., 1976. Biogeochemistry and bacteriology of ferrous iron oxidation in geothermal habitats. Geochim. Cosmochim. Acta 40, 493-500.

Celik, M., 1999. Minamiite and alunite occurrences formed from volcanic emanations, West-Southwest of Konya, Turkey. Geol. Bull. Turkey 42, 89-97.

Cleverley, J.S., Benning, L.G., Mountain, B.W., 2003. Reaction path modeling in the As-S system: a case study for geothermal As transport. Appl. Geochem. 18, 1325-1345.

Craig, H., 1961. Isotopic variations in meteoric waters. Science 133, 1702-1703.

Craig, H., Gordon, L.I., Horibe, Y., 1963. Isotopic exchange effects in the evaporation of water. J. Geophys. Res. 68, 5079-5087.

Criss, R.E., Taylor, H.P. Jr., 1986. Meteoric-hydrothermal systems. In: P.H. Ribbe (Ed)., Stable Isotopes in High Temperature Geologic Processes, Min. Soc. Am. Reviews in Min. 16, 165-181.

Delmelle, P., Bernard, A., Kusakabe, M., Fischer, T.P., Takano, B., 2000. Geochemistry of the magmatic-hydrothermal system of Kawah Ijen volcano, East Java, Indonesia. J. Volcanol. Geotherm. Res. 97, 31-53.

Dymkina, V.A., Solomonov, V.A., Karpov, G.A., 1988. Peculiarities of the composition of spontaneous gases from the Uzon Caldera analyzed directly in the thermal field. Geologiya i Geofizika 29, 42-47.

Ellis, A.J., Mahon, W.A.J., 1967. Natural hydrothermal systems and experimental hot water/rock interactions (Part II). Geochim. Cosmochim. Acta 31, 519-538.

Epstein, S., Mayeda, T., 1953. Variation of O^{18} content of waters from natural sources. Geochim. Cosmochim. Acta 4, 213-224.

Eroshchev-Shak, V.A., Karpov, G.A., Il'in, V.A., 1985. Lithology of the modern sediments of Chloride Lake in Kamchatka. Litol. Polezn. Iskop. 1, 35-48.

Field, C.W., Fifarek, R.H., 1985. Light stable-isotope systematics in the epithermal environment. In: B.R. Berger, P.M. Bethke (Eds)., Geology and Geochemistry of Epithermal Systems, Soc. Econ. Geol. Reviews in Econ. Geol. 2, 99-128.

Fliermans, C.B., Brock, T.D., 1972. Ecology of sulfur-oxidizing bacteria in hot acid soils. J. Bacteriol. 111, 343-350.

Giggenbach, W.F., 1978. The isotopic composition of waters from the El Tatio geothermal field, Northern Chile. Geochim. Cosmochim. Acta 42, 979-988.

Giggenbach, W.F., 1987. Redox processes governing the chemistry of fumarolic gas discharges from White Island, New Zealand. Appl. Geochem. 2, 143-161.

Giggenbach, W.F., 1997. The origin and evolution of fluids in magmatic-hydrothermal systems. In: H.L. Barnes (Ed)., Geochemistry of Hydrothermal Ore Deposits, 2nd ed. J. Wiley and Sons, New York, 509-567.

Giggenbach, W.F., and Goguel, R.L., 1989. Collection and analysis of geothermal and volcanic water and gas discharges. Department of Scientific and Industrial Research, Chemistry Division, Petone, NZ, 4th ed. Rept. CD 2401, 1-81.

Goff, F., Gardner, J., Vidale, R., Charles, R., 1985. Geochemistry and isotopes of fluids from sulphur

springs, Valles Caldera, New Mexico. J. Volcanol. Geotherm. Res. 23, 273-297.

Hedenquist, J.W., 1991. Boiling and dilution in the shallow portion of the Waiotapu geothermal system, New Zealand. Geochim. Cosmochim, Acta 55, 2753-2765.

Hoog, J.M.C., Taylor, van Bergen, M.J., 2001. Sulfur isotope systematics of basaltic lavas from Indonesia: implications for the sulfur cycle in subduction zones. Earth and Planet. Sci. Lett. 189, 237-252.

Karpov, G.A., 1995. Post-session field trip to kamchatka: part II Uzon Geyser Depression. In: Proc. 8th Intern. Symposium on Water-Rock Interaction-WRI-8, Aug. 15-19, Vladivostok, Russia, Aug.15- Aug.19.

Karpov, G.A., 1998. Uzon: A Protected Land. M.: Logata, Moscow.

Karpov, G.A., 2005. Geothermal and mineral resources in modern volcanism areas. In: Proc. of the Intern. Field Kurile-Kamchatka Seminar, July 16- Aug. 6, Petropavlovsk-Karmchatsky, 74-88. (in Russian)

Karpov, G.A., Naboko, S.I., 1990. Metal contents of recent thermal waters, mineral precipitates and hydrothermal alteration in active geothermal fields, Kamchatka. J. Geochem. Explor. 36, 57-71.

Kusakabe, M., Komoda, Y., Tokano, B., Abiko, T., 2000. Sulfur isotopic effects in the disproportionation reaction of sulfur dioxide in hydrothermal fluids: Implications for the $\delta^{34}S$ variations of dissolved bisulfate and elemental sulfur from active crater lakes. J. Volcanol. Geotherm. Res. 97, 287-307.

Kyser, T.K., 1987. Equilibrium fractionation factors for stable isotopes. In: T. K. Kyser (Ed)., Stable Isotope Geochemistry of Low Temperature Fluids, Min. Assoc. Can. Short Course Notes 13, 1-84.

Marini, L. Gambardella, B., Principe, C. Arias, A., Bromback, T., Hunziker, J.C., 2002. Characterization of magmatic sulfur in the Aegean island arc by measurement of the $\delta^{34}S$ values of fumarolic H_2S, elemental S, and hydrothermal gypsum from Nisyros and Milos islands. Earth

Planet. Sci. Lett. 200, 15-31.

Migdisov, A.A., Dadze, T.P., Gerasimovskaya, L.A., 1991. Forms of sulfur in the ore-bearing hydrothermal solutions of Uzon Caldera (Kamchatka). Geokhimiya 12, 1682-1691.

Millero, F.J., 1986. The thermodynamics and kinetics of the hydrogen sulfide system in natural waters. Marine Chem. 18, 121-147.

Moore, D.M., Reynolds, R.C.Jr., 1997. X-Ray Diffraction and the Identification and Analysis of Clay Minerals, 2nd ed. Oxford University Press, New York.

Mosser, J.L, Mosser, A.G., Brock, T.D., 1973. Bacterial origin of sulfuric acid in geothermal habitats. Science 179, 1323-1324.

Ohmoto, H., Goldhaber, M.B., 1997. Isotopes of sulfur and carbon. In: H.L. Barnes (Ed)., Geochemistry of Hydrothermal Ore Deposits, 2nd ed. J. Wiley and Sons, New York, 509-567.

Pritchard, M.E., Simmons, M., 2004. Surveying volcanic arcs with satellite radar interferometry: the Central Andes, Kamchatka, and Beyond. GSA Today 14, 4-11.

Rafter, T.A., Kaplan, I.R., Hulston, J.R., 1960. Sulphur isotopic variations in nature: Part 7 – Sulphur isotopic measurements on sulphur and sulphates in New Zealand geothermal and volcanic areas. N.Z. J. of Sci., 3, 209-218.

Reyes, A.G., Vickridge, I.C., 1996. Distribution of lithium, boron, and chloride between fresh and altered rocks in the Kawerau geothermal system, New Zealand. In: S.F. Simmons, M.M. Rahman and A. Watson (Eds)., Proc. of the 18th N.Z. Geoth. Wkshp., 18, 121-126.

Rye, R.O., 1993. SEG distinguished lecture: the evolution of magmatic fluids in the epithermal environment: the stable isotope perspective. Econ Geol. 88, 733-753.

Sakai, H., 1968. Isotopic properties of sulphur compounds in hydrothermal processes. Geochem. J. 2, 29-49.

Seal, R.R., Alpers, C.N., Rye, R.O., 2000. Stable isotope systematics of sulfate minerals. In: C.N. Alpers, J.L. Jambor (Eds)., Sulfate Minerals-crystallography, geochemistry, and environmental

significance, Min. Soc. Am. Geochem. Soc. Reviews in Min. and Geochem. 40, 541-593.

Szaran, J., 1996. Experimental investigation of sulphur isotopic fractionation between dissolved and gaseous H_2S. Chem. Geol. 127, 223-228.

Sheppard, D.S., Lyon, G.L., 1984. Geothermal fluid chemistry of the Orakeikorako field, New Zealand. J. Volcanol. and Geotherm. Res. 22, 329-349.

Sheppard, S.M.F., 1986. Characterization and isotopic variations in natural waters. In: P.H. Ribbe (Ed)., Stable Isotopes in High Temperature Geologic Processes, Min. Soc. Am. Reviews in Min. 16, 165-181.

Shoen, R., Rye, R.O., 1970. Sulfur isotope distribution in solfataras, Yellowstone National Park. Science 170, 1082-1084.

Socki, R.A., Karlsson, H.R., Gibson Jr., E.K., 1992. Extraction technique for the determination of oxygen-18 in water using pre-evacuated glass vials. Anal. Chem. 64, 829-831.

Spirakis, C. S., 1984. Effect of sulfur kinetics on redox reactions and implications for the genesis of epithermal ore deposits. In: T.V. Janelidze, A.G., Tvalchrelidze (Eds)., Proc. of the 6th Quadrennial IAGOD Symp., Intern. Assoc. Genesis Ore Dep. 1, 201-203.

Ueda, A., Sakai, H., 1984. Sulfur isotope study of Quaternary volcanic rocks from the Japanese Islands Arc. Geochim. Cosmochim. Acta 48, 1837-1848.

Varekamp, J.C., Kruelen, R., 2000. The stable isotope geochemistry of volcanic lakes, with examples from Indonesia. J. Volcanol. and Geotherm. Res. 97, 309-327.

Waltham, 2001. A guide to the volcanoes of southern Kamchatka, Russia: Proc. of the Geologists' Assoc. 112, 67-78.

White, D.E., Muffler, L.J.P., and Truesdell, A.H., 1971. Vapor dominated hydrothermal systems compared with hot-water systems. Econ. Geol. 66, 75-97.

Zinder, S., Brock, T.D., 1977. Sulfur dioxide in geothermal waters and gases. Geochim. Cosmochim. Acta 41, 73-79.

APPENDIX A

RESULTS OF EXPERIMENTAL METHOD TESTS

Table showing the $\delta^{34}S$ isotope values of S-bearing minerals extracted from rock, core, and water samples according to a variety of separation and sample preservation methods. Included are the results for procedures using:

1. A warm, agitated acetone bath to dissolve elemental sulfur from other S-bearing mineral phases for a 48h period with subsequent filtering off the S^0-bearing acetone aliquot. Once the aliquot has been separated, the acetone is allowed to evaporate resulting in re-precipitation of the elemental sulfur component for analysis.

2. An oven set at 150°C temperatures to sublimate elemental sulfur from sulfur/pyrite mixtures, therefore isolating the pyrite for analysis.

3. Acidified vs. non-acidified water samples taken during the field collection process to determine whether either sampling method alters the sulfur isotopic signature of the aqueous sulfate.

Appendix A, Table 1
Results of experiments investigating the validity of mineral separation methods and sample usage for $\delta^{34}S$ analysis.

Experiment and Sample Name	Sample no.	$\delta^{34}S$ (‰)	Additional Parameters		Conclusion
Acetone Separation of Elemental Sulfur					
Sample Name	#	For S			
Original pure elemental sulfur stock	CL1-302-2	5.3			Not a suitable method for this study.
Sulfur precipitated w/filter	CL1-302-3	5.7			
Sulfur precipitated wo/filter	CL1-302-4	6.6			
S experiment 3	CL2-12-5	5.2			
Pure elemental sulfur stock duplicate	CL2-1-2	5.0			
Pyrite Oxidation/Sublimation					
Sample Name	#	For Pyrite			
pyrite stock	CL2-1-5	2.6			Appropriate method for this study.
microned pyrite stock	CL2-1-4	2.8			
150°C microned pyrite for 24hrs	CL2-1-3	3.0			
Tri experiment (S/pyr/kaol) then S sublimated	CL2-2-5	3.0			
Sulfate for Acidified vs. Non Acidified Waters					
Sample Name	#	For Sulfate	Sulfate Concentration		
No acid	CJ-61	-0.1	Medium		Both acidified and non-acidified samples for a variety of sulfate concentrations can be used for aqueous sulfate S isotopic analysis in this study.
Acid	CJ-62	-0.6	Medium		
No Acid	CJ-21	-1.2	High		
Acid	CJ-22	-1.0	High		
No acid	CJ-05	-0.2	Medium		
Acid	CJ-06	-0.1	Medium		
No acid	CJ-45	3.6	Low		
Acid	CJ-46	3.8	Low		
No acid	CJ-17	-0.3	Medium		
Acid	CJ-18	-0.1	Medium		

APPENDIX B

XRD DATA USED IN INTERPRETING MINERALOGY FOR SAMPLES

The following tables summarize the results of the XRD analysis for all samples collected during the 2003 expedition:

Table 1: XRD data for rock samples

Table 2: XRD data for core and sinter/sediment samples

The following figures are XRD patterns of select samples. Figures 1-2 are patterns that demonstrate the basic XRD techniques used in interpreting the mineralogy of samples, Figures 3-7 are patterns representing the most common mineral assemblages found throughout the caldera. A complete library of patterns can be requested on CD from a data repository at the University of Georgia (contact Dr. Douglas Crowe, crowe@gly.uga.edu).

Figure 1: Ethylene glycolation of dc03-68silt

Figure 2: Sulfur sublimation of dc03-023silt

Figure 3: Dc-026silt mineral assemblage

Figure 4: Dc-068silt mineral assemblage

Figure 5: Dc-010silt mineral assemblage

Figure 6: Erh-015 mineral assemblage

Figure 7: Erh-30worwa mineral assemblage

Appendix B, Table 1

Interpretation of XRD data for the complete list of rock samples collected[a]. Only the underlined, S-bearing mineral samples were used in this study.

Sample no.	Sample Name	Location[b]	Mineral Species Present [c d]															
			And	Plg	Px	OpA	OpCT	OpC	Qtz	K	Sulf	Jar	Py	Feox	Mn	Br	Md	UIP
erh-053	Tripool	EETF	x			xxx												
erh-054	Tripool	EETF	xx			xxx												
erh-055	Tripool	EETF									xxxx							
erh-056	Thermophile	EETF				xxx			xx									
erh-057	Thermophile	EETF	xx			xxx												
erh-058	Midfield	EETF	x			xxx			xx	xx								
erh-059	Midfield	EETF	xxx			x												
erh-060	Cleft Pool	EETF	xxx			xx												
erh-061	Zavarzin Pool	EETF				xxx							xx					
erh-062	Zavarzin Pool	EETF				xxx												
erh-063	Cleft Pool	EETF				xxx												
erh-001	Near U Pool	CETF				xxx			x									
erh-002	Near U Pool	CETF												xxxx				
erh-003	Near U Pool	CETF				xxx			x									
erh-004	Pool N. of Arkashin	CETF																
erh-005	Near Arkashin	CETF	xxx		x	xx			x									x
erh-006	16 M Well	CETF																
erh-008	Ultino/Borlashy	WETF	xxx					x										
erh-040	JK Pool Area	CETF	xxx			xxx			xx									
erh-041	JK Pool Area	CETF									xxxx							
erh-042	JK Pool Area	CETF	xxx		x													
erh-043	JK Pool Area	CETF	x			xxx			x									
erh-044	JK Pool Area	CETF				xxxx												
erh-045	JK Pool Area	CETF	x			xxx			x									
erh-046	JK Pool Area	CETF					xxx		xx									
erh-047	JK Pool Area	CETF	xxx			xxx												

Appendix B, Table 1
Continued

Sample no.	Sample Name	Location[b]	Mineral Species Present [c d]															
			And	Plg	Px	OpA	OpCT	OpC	Qtz	K	Sulf	Jar	Py	Feox	Mn	Br	Md	UIP
erh-069	Kloridnoe Lake	CETF																
erh-070	Bright White	CETF				xxx		xx	xx									x
erh-065	Eight Lake	CETF				x		xx	xx								xx	x
erh-066	Eight Lake	CETF															xxxx	
erh-067	Eight Lake	CETF				xxx				xx	xx	xx						
erh-009	General Select	OTF							xxxx	o								
erh-010	General Select	OTF							xxxx	o								
erh-011a	Rind subsample	OTF				xxx		x	xx	xx								
erh-011b	Inside subsample	OTF				xxx		x	xx	xx								
erh-012	General Select	OTF						xxx	xx	xx								
erh-013	General Select	OTF							xxx	xx								
erh-014	General Select	OTF							xxx	xxx								
erh-015	General Select	OTF						xx	xx			xxx	x					
erh-016a	A subsample	OTF						xxx	xx	xx	o							
erh-016b	B subsample	OTF							xxxx	o								
erh-017	General Select	OTF						xxx	xx	xx								
erh-018	General Select	OTF						xxx	x	xx	xx							
erh-019	General Select	OTF						xx	xxx			xxx	x					
erh-020	General Select	OTF						xxx	x									
erh-021	Gen. Select rock fall	NTF	xxx		x													
erh-022	Gen. Select rock fall	NTF	xxx		x									x				
erh-023	Gen. Select rock fall	NTF	xxx		x									x				
erh-024	Gen. Select rock fall	NTF	xxx			x								xxx				
erh-025	Gen. Select rock fall	NTF	xxx															
erh-026	Gen. Select rock fall	NTF	xxx			x								x				
erh-027	Gen. Select entrance	NTF	xxx		x													
erh-048	General Select	WTF	xxx			xx												
erh-049	General Select	WTF				xx		x						xxx				x

Appendix B, Table 1
Continued

Sample no.	Sample Name	Location[b]	Mineral Species Present [c d]															
			And	Plg	Px	OpA	OpCT	OpC	Qtz	K	Sulf	Jar	Py	Feox	Mn	Br	Md	UIP
erh-050	General Select	WTF							xxx	xxx								x
erh-051	General Select	WTF	xxx											x				
erh-052	General Select	WTF									xxxx							
erh-xtra (3sub)	General Select	WTF							o			xx				xxx		
erh-028	Stream Bank	MTB	xxx			xxx												
erh-030-worwa	WOR Slope	MTB				xxx									xxx			
erh-030-worwb	WOR Slope	MTB				xxx									xxx			
erh-031-woro1	WOR Slope	MTB		xx		xxx									xx			
erh-031-woro2	WOR Slope	MTB		xxx		xx												
erh-031-woro3	WOR Slope	MTB				xx				x					xx			
erh-031-woro4	WOR Slope	MTB				xx									xx			
erh-032-worr1	WOR Slope (3sub)	MTB	xx			xxx									xxx			x
erh-032-worr3	WOR Slope	MTB	xxx															
erh-033	1st drainage bynd	MTB	xxx			xx		x										
erh-034	1st drainage bynd	MTB	xxx			xx												
erh-035	2nd drainage bynd	MTB	xx			xxx				xxx								
erh-036	General Select	LMR	xxxx															
erh-037	General Select	LMR	xxxx															
erh-038	General Select	LMR	xxxx															
erh-maar1	General Select	LMR	xxx		x					o								
erh-maar2	General Select	LMR	xxx		x													
erh-039	1st confluence after	LMR	xxx		x													

[a] Analytical methods as follows: XRD (UGA).

[b] East Sector of East Thermal Field (EETF); Central Sector of East Thermal Field (CETF); Orange Thermal Field (OTF); North Thermal Field (NTF); West Thermal Field (WTF); Mount Belaya (MTB); Maar Lake Dalnee (LMR).

[c] Mineral abbrev. are as follows: Andesite (And); Other Plagioclase species (Plg); Pyroxene (Px); Opals (OpA, OpCT, OpC); Quartz (Qtz); Kaolin group minerals (K); Elemental Sulfur (Sulf); The alunite group mineral Jarosite (Jar); Pyrite (Py); Varieties of iron oxy hydroxides (Feox); The alunite group mineral Minamiite (Mn); Brushite (Br); Mordenite (Md); Any unidentified peaks present (UIP).

[d] The symbols denoting the amount of the mineral in the sample are as follows: (XXXX) the mineral composes the entire sample; (XXX) the mineral composes a majority of the sample; (XX) the mineral composes a portion of the sample; (X) the mineral is a minor component of the sample; (o) The mineral is found only in trace amounts.

Appendix B, Table 2
Interpretation of XRD data for the complete list of core samples and sinter/sediment samples collected. Only the underlined, S-bearing mineral samples were used in this study.

Sample no.	Sample Name	Size Fraction	Tests Run[a]	Mineral Species Present[bc]										
				And	OpA	Qtz	K	Smc	Sulf	Jar	Py	Real	Poss. Min.	UIP[d]
dc-018	EETF Zavarzin	Clay	air, eth, heat series		x	o	x	x	xxx					
dc-018	EETF Zavarzin	Silt	air, eth, 150°C	o	o	o			xxx		o			
dc-019	EETF Zavarzin	Clay	air, eth, heat series		x	o	x	xx	xxx					o
dc-019	EETF Zavarzin	Silt	air, eth		x			xx	xxx		o			o
dc-019a	EETF Zavarzin	Clay	air, eth, heat series		x	o	x	xx			xx			o
dc-019a	EETF Zavarzin	Silt	air, eth	o	x	x	o	xx			xxx			o @21
dc-020	EETF Zavarzin	Clay	air, eth, heat series		x	o	xx	x			xx			o
dc-020	EETF Zavarzin	Silt	air, eth	x	x	x	o				xxx			
dc-021	EETF Tripool	Clay	air, eth		x		x	x	xxx		x			o
dc-021	EETF Tripool	Silt	air						xxxx					
dc-022	EETF Tripool	Clay	air, eth		x		x		xx		x			o
dc-022	EETF Tripool	Silt	air, eth, 150°C	o	x	o	o		xxx		o			
dc-023	EETF Tripool	Clay	air		x		xx	xxx	o		x			o
dc-023	EETF Tripool	Silt	air, 150°C	o	o	o	o		xxxx		o			o
dc-068	EETF Cleft Bulk	Clay	air, eth			x	x	xxx	xx		x			
dc-068	EETF Cleft Bulk	Silt	air, eth				o	x	xxx		xx			
dc-015	CETF Jp vent	Clay	air, eth				xxx	xx						o @21
dc-015	CETF Jp vent	Silt	air, eth	xx		x	xxx	x	x					o @21
dc-016	CETF Jp vent	Clay	air, eth				xxx	xx						o @21
dc-016	CETF Jp vent	Silt	air, 150°C	xx	x	x	xxx	x			x			o @21
dc-017	CETF Jp vent	Clay	air, eth				xxx	xx						
dc-017	CETF Jp vent	Silt	air, eth	xx	o	x	xxx	x			x			o @21
dc-024	CETF Shovel	Clay	Missing											
dc-024	CETF Shovel	Silt	air, eth	xx			xx	x			xxx			o @ 11
dc-025	CETF Shovel	Clay	Missing											

Appendix B, Table 2
Continued

Sample no.	Sample Name	Size Fraction	Tests Run[a]	Mineral Species Present[bc]										
				And	OpA	Qtz	K	Smc	Sulf	Jar	Py	Real	Poss. Min.	UIP[d]
dc-025	CETF Shovel	Silt	Missing											
dc-026	CETF Shovel	Clay	Missing											
dc-026	CETF Shovel	Silt	air, eth	xx			x	o				xxx		o
dc-027	CETF Shovel	Clay	air						x		x			
dc-027	CETF Shovel	Silt	air, eth	xx			x					x		o
dc-028	CETF Shovel	Clay	Missing											
dc-028	CETF Shovel	Silt	air, eth	xx			x	x			xxx	x		o @ 11
dc-029	CETF 13 m SE K4	Clay	air, eth			o	xxx	x	x		x			
dc-029	CETF 13 m SE K5	Silt	air	xx		x	xx	x			xx			o
dc-8lake	8lake mudpot	Clay	air, eth				xxx	x						o @21
dc-8lake	8lake mudpot	Silt	air		x	x	xxx	o						o @21
dc-010	WTF sed/crust	Clay	air, eth		o		xx	xx			xx			o
dc-010	WTF sed/crust	Silt	air, eth			x	xx	x		xx	xxx			o @ 11
cr-022	EETF cleft pool	bulk	air, 150°C	x	x	o	x	o		xx	x			
cr-009	EETF Lake Bannoe	bulk	air						xxx		xx			
cr-016	CETF bright white	bulk	air, 150°C						xxx					o
cr-029	EETF Yllwsputter	bulk	air						xxxx					
cr-041	hotblack pool	bulk	air, eth	x	x	x					x			o
cr-sinter	CETF bright white	bulk	airblk	xx									Gypsum	o

[a] Tests Run include: air dried sample (air); ethylene glycol solvation (eth); sublimating sulfur at 150°C (150°C); heat treatment series includes baking the sample at 100°C, 350°C, and 550°C temperatures for 24 h periods.

[b] Mineral abbrev. are as follows: Andesine (And); Opal A (OpA);Quartz (Qtz); Kaolin group minerals (K); Smectite (Smc);Elemental Sulfur (Sulf); The alunite group mineral Jarosite (Jar); Pyrite (Py); Realgar (Real); Other possible minerals (Poss. Min.); Any unidentified peaks present (UIP).

[c] The symbols denoting the amount of the mineral in the sample are as follows: (XXXX) the mineral composes the entire sample; (XXX) the mineral composes a majority of the sample; (XX) the mineral composes a portion of the sample; (X) the mineral is a minor component of the sample; (o) The mineral is found only in trace amounts.

[d] Those samples with potentially the same unidentified mineral had the 2Θ degree of the strongest unidentified peak listed.

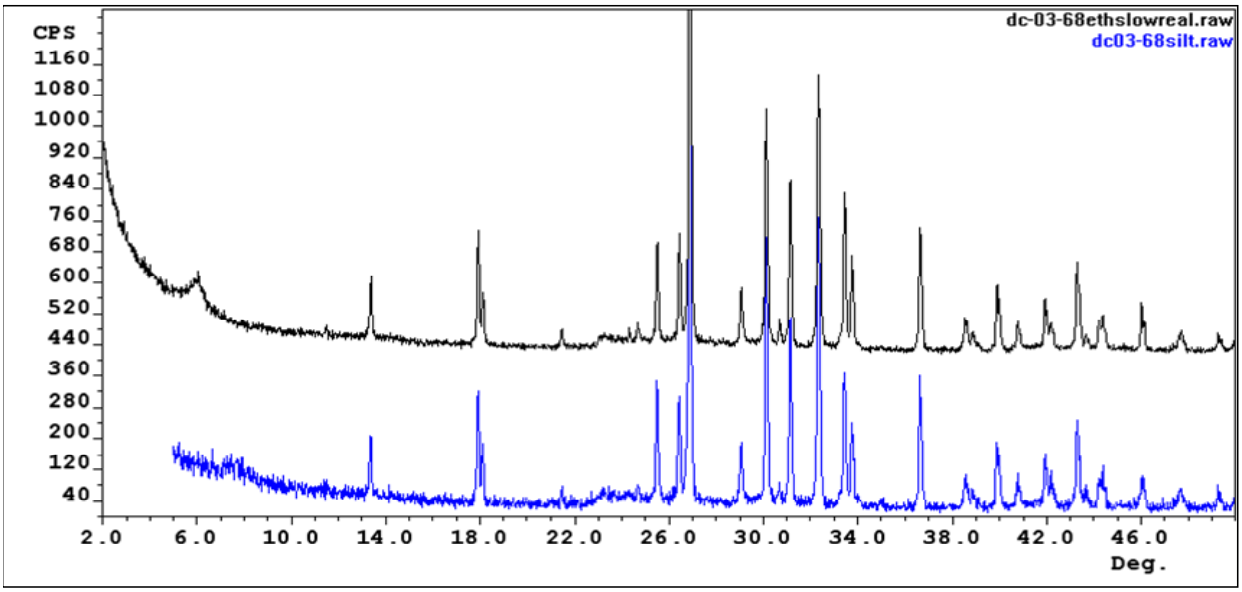

Appendix B, Fig. 1. Comparison of two separate runs of dc03-68silt before (bottom) and after (top) ethylene glycol solvation. Note the promanent shift to the left of the initially inconspicuous 7° 2Θ peak as the smectite component expands in the sample.

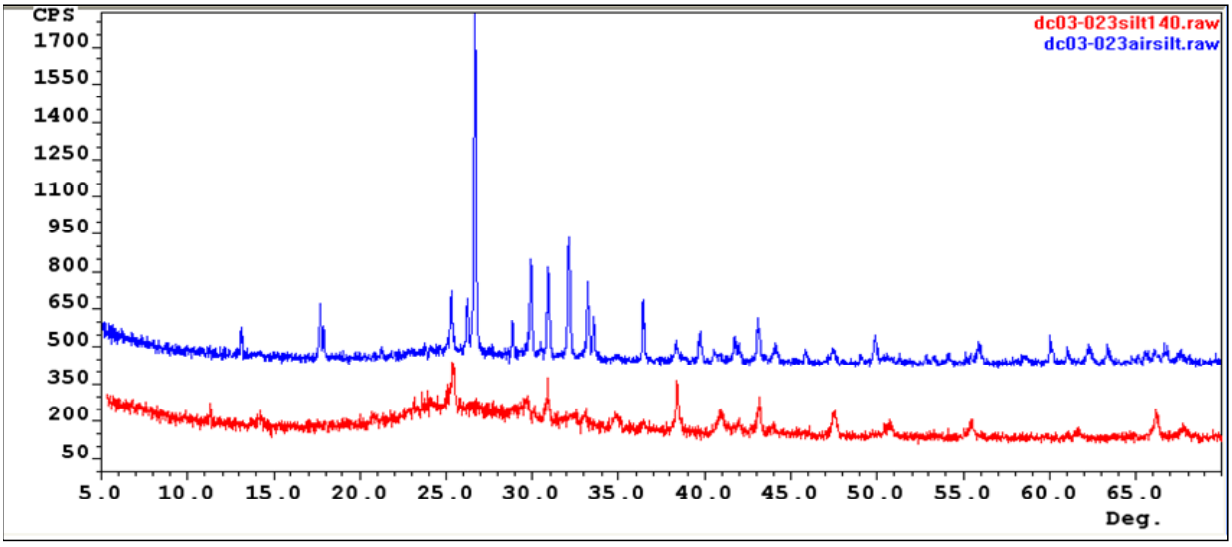

Appendix B, Fig. 2. Comparison of two separate runs of dc03-023silt before (top) and after (bottom) heating at 150°C for a 24h period. Note the dissapearance of the peaks associated with the sulfur prior to sublimation, thus allowing peaks associated with the more discreate phases present to become visible.

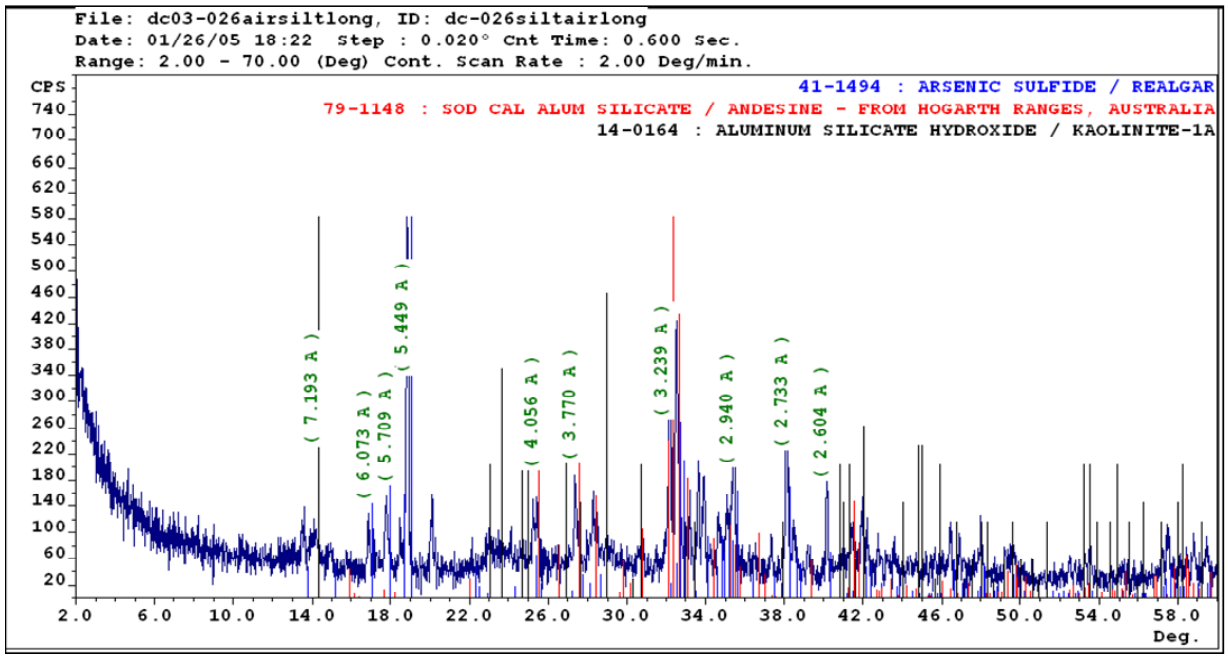

Appendix B, Fig. 3. Sample dc-026silt demonstrates the pattern generated by a common mineral assemblage found in the ore zone of the CETF that includes realgar, andesine, and kaolinite.

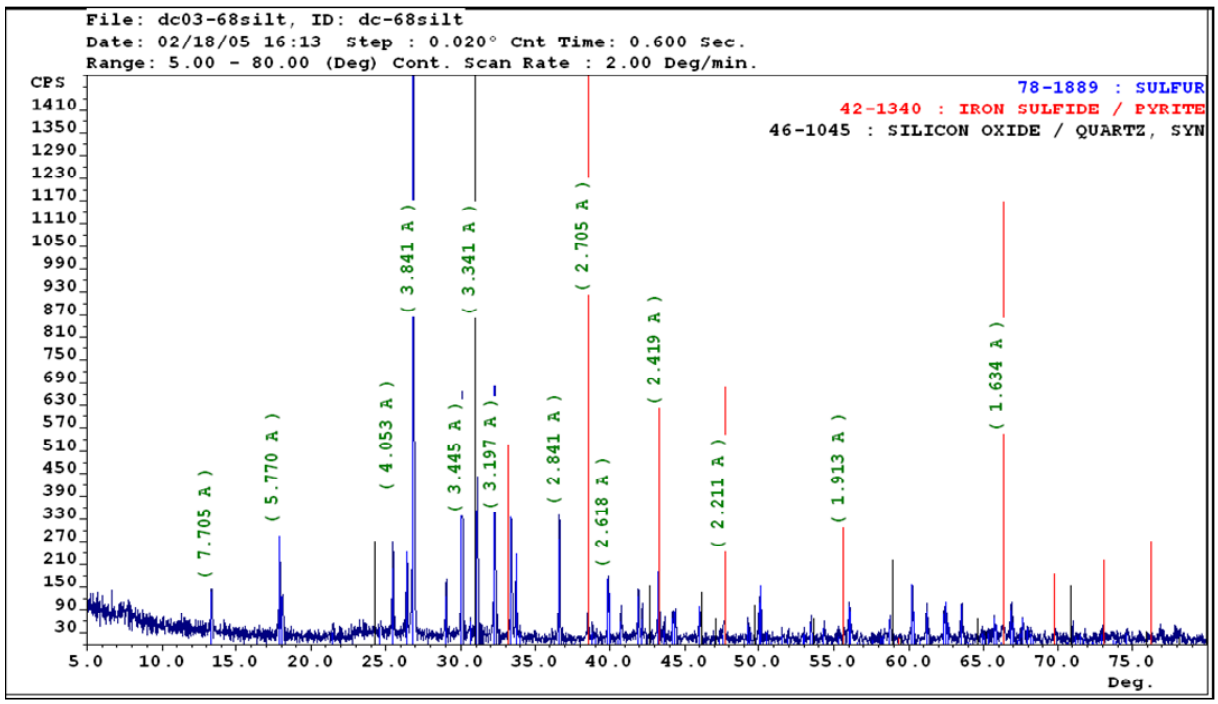

Appendix B, Fig. 4. Sample dc-68silt demonstrates the pattern generated by a common mineral assemblage found throughout the caldera that includes quartz, pyrite, and sulfur.

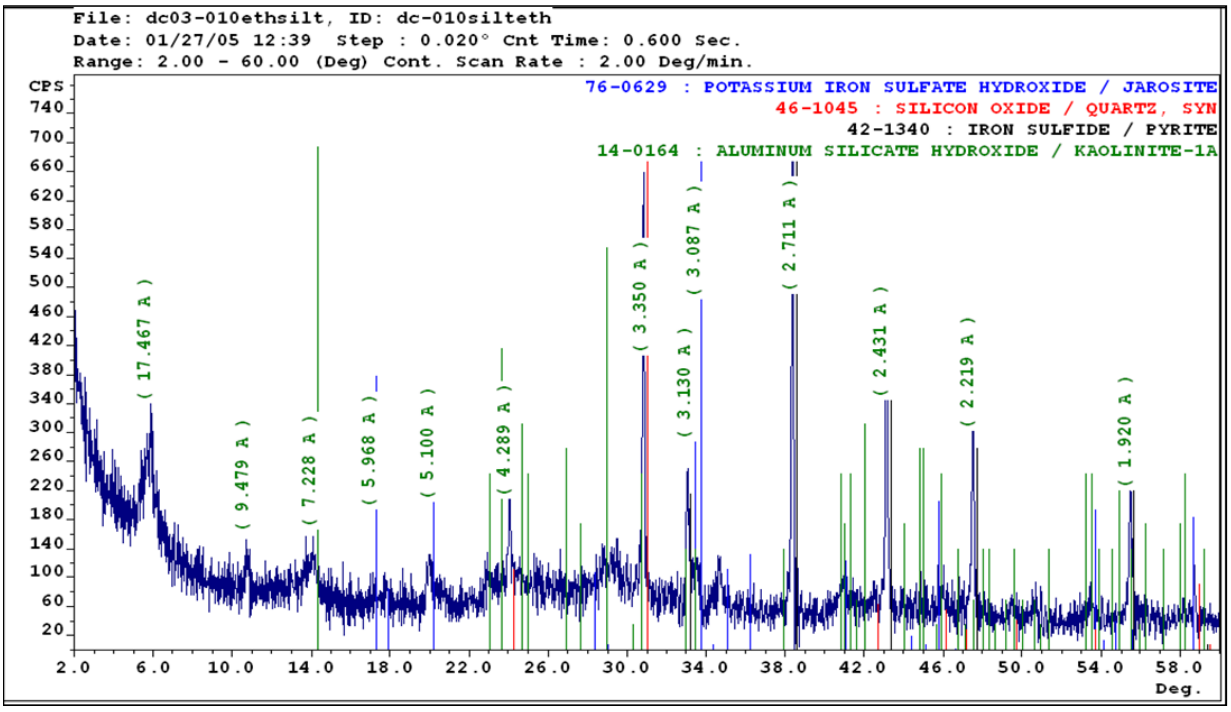

Appendix B, Fig. 5. Sample dc-010silt demonstrates the pattern generated by a common mineral assemblage found throughout acidic areas within the caldera that includes quartz, pyrite, kaolinite, and jarosite.

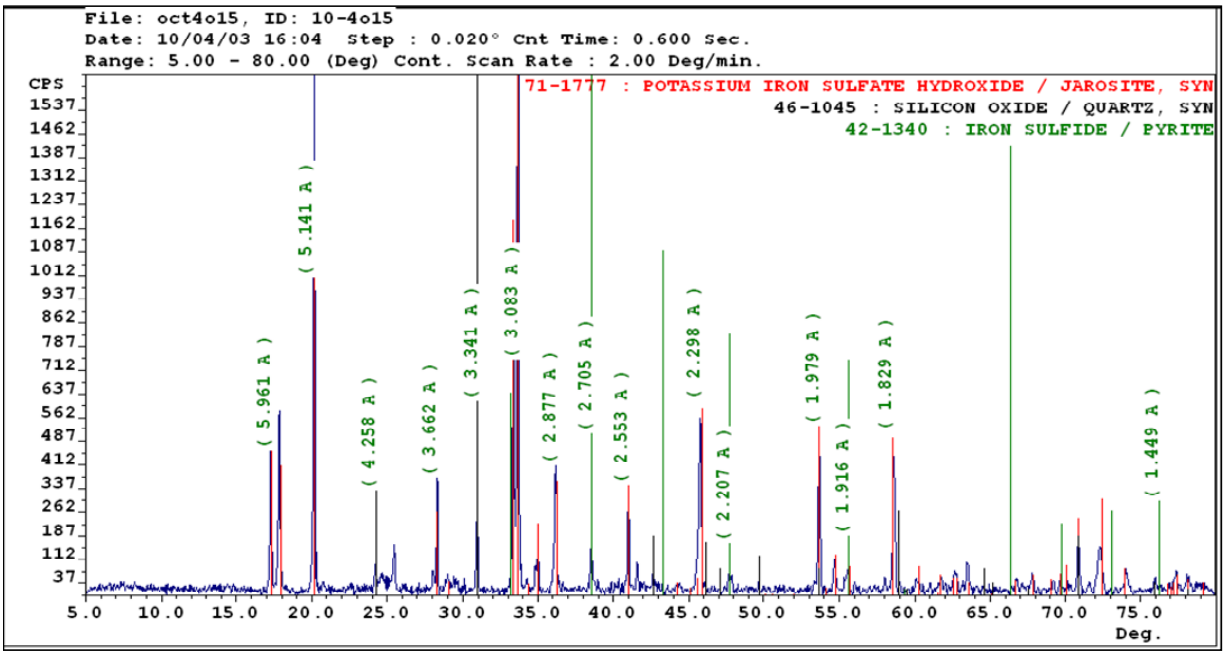

Appendix B, Fig. 6. Sample erh-015 demonstrates the pattern generated by a common mineral assemblage found within rocks in acidic zones throughout the caldera that includes quartz, pyrite, and jarosite, with Opal-CT (at 24-26° 2Θ).

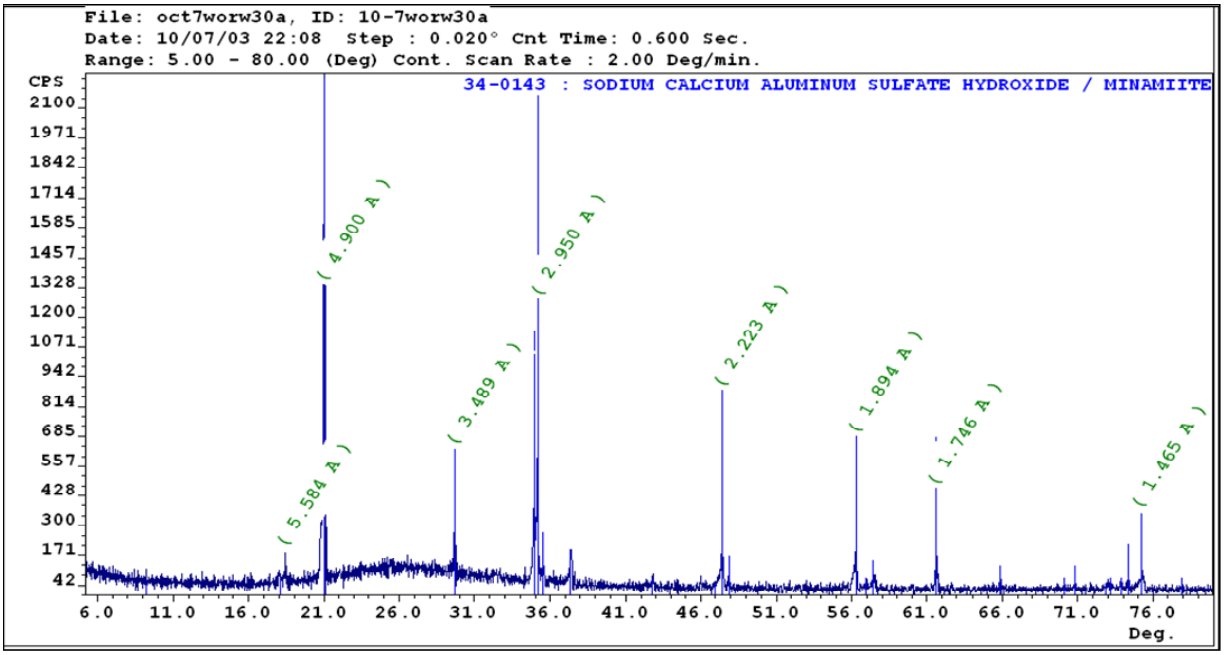

Appendix B, Fig. 7. Sample erh-30worwa demonstrates the pattern generated by the mineral assemblage found within the acid sulfate altered rocks of Mt. Belaya that includes minamiite with 0pal-A (amorphous hump at 21-36° 2Θ).

APPENDIX C

DETAILED LOG OF SULFUR ISOTOPE DATA FOR ALL SAMPLES

The following tables show the $\delta^{34}S$ isotope values of the S-bearing species extracted from water, rock, and core samples with duplicate runs included. A complete log of isotope work can be requested from the Department of Geology's Stable Isotope Lab at the University of Georgia (contact Mrs. Julia Cox, jcox@gly.uga.edu).

Table 1: $\delta^{34}S$ of aqueous sulfate from water samples

Table 2: $\delta^{34}S$ of S-bearing minerals extracted from rock samples

Table 3: $\delta^{34}S$ of S-bearing minerals extracted from core and sinter/sediment samples

Appendix C, Table 1
Data from sulfur isotope analysis of aqueous sulfate.

Sample no.	Sample Name	$\delta^{34}S$ Acidified (‰)	$\delta^{34}S$ Unacidified (‰)	Notes
DC03-007	Small easternmost pool (WTF)	0.3		
CJ03-020	center pool (OTF)	-0.3		
CJ03-046	3 M pool 75 m east of thermophile pool (ETF)	3.8	3.6	
CJ03-006	Mosha's Pool (CETF)	-0.1	-0.2	
CJ03-018	clear pond across orange island (OTF)	-0.3	-0.1	
CJ03-062	NE corner down slope from observation deck (EETF)	-0.6	-0.1	
CJ03-022	mud pit (OTF)	-1.0	-1.2	
DC03-012	Very active High T vent (WTF)	0.0		
CJ03-014	Borlyashchy Pool (CETF)	4.1		
CJ03-066	Spectacles Pool (CETF)	13.2		Combined both samples
CJ03-042	East pools of Chloride lake (EETF)	3.7		
DC03-005	Lowermost large pool (WTF)	0.2		
DC03-003	Small black sandy bubbler 8m N of Vent 1 (JK)	3.4		
CJ03-002	Arkashin (CETF)	7.6		Combined both samples
CJ03-008	Masha's Pool (CETF)	-0.1		
CJ03-010	Just N of Arkashin (CETF)	0.0		
CJ03-048	Data logger pool near Bannoe pool (EETF)	6.2		Combined both samples
CJ03-054	across land bridge from Cleft (EETF)	1.9		
JK03-015	Khloridnoe Lake (CETF)	3.8		
CJ03-052	Cleft Pool (EETF)	2.3		
JK03-013	Vent 2 (JK)	2.8		
CJ03-036	Maar Lake (LMR)			
CJ03-050	Zavarzin Pool (EETF)	8.0		
JK03-014	94°C pool by Jen's Pools(same outflow) (JK)	2.7		Combined both samples
JK03-012	Vent 1 (JK)	4.2 and 4.2		Combined both samples
DC03-001	Vent 1 (JK)			

Appendix C, Table 1
Continued

Sample no.	Sample Name	$\delta^{34}S$ Acidified (‰)	$\delta^{34}S$ Unacidified (‰)	Notes
CJ03-056	Lake Bannoe (EETF)			
CJ03-060	Shark's Noses fishing stream (STMS)			
CJ03-064	bright white outflow into chloride lake (CETF)			
CJ03-024	first deep blue pool (NTF)			
CJ03-040	Stream parallel to Maar rim (STMS)			
CJ03-032	WOR stream (STMS)			
CJ03-044	Thermophile spring (EETF)			
CJ03-026	small yellow pond (NTF)			
CJ03-030	Stream draining Mt. Belaya (STMS)			
CJ03-016	at campsite (STMS)			
CJ03-028	gray filamentous pool (NTF)			
CJ03-038	at headwaters (STMS)			
CJ03-012	16M well (CETF)	8.6		Combined both samples
CJ03-004	Sunlight Spring (WETF)			

Appendix C. Table 2
Data from sulfur isotope analysis of rock samples. Only the underlined samples were applicable to this study.

Sample no.	Sample Name	Mineral δ34S (‰)				
		Pyrite	Sulfur	Jarosite	Minamiite	Notes
erh-015	Orange Springs	x		xxx		Unable to separate
erh-016	Orange Springs		Minor			
erh-018	Orange Springs		1.8 and 1.7			
erh-019	Orange Springs	x		xxx		Unable to separate
erh-030-worwa	WOR Slope				-5.05	
erh-030-worwb	WOR Slope				-3.1	
erh-031-woro1	WOR Slope				-0.35	
erh-031-woro3	WOR Slope				-4.9	
erh-031-woro4	WOR Slope				-3.43	
erh-032-worr1	WOR Slope				-5.19 and -5.24	
erh-041	JK Pools		0.5			
erh-047	JK Pools	-3.8 and-3.9				
erh-49	WTF					
erh-052	WTF		1.3			
erh-xtra	WTF				2.06 and 1.6	
erh-055	ETF Tripool		-1.5			
erh-067	Eight Lake		-3.4 and 0.3			

Appendix C, Table 3
Data from sulfur isotope analysis of core and sinter/sediment samples. Only the underlined samples were used in this study.

Gravel Sized Fraction

Sample no.	Sample Name	Mineral δ34S (‰)		
		Pyrite	Realgar	Notes
dc-010	WTF sed/crust	-0.9		
dc-015	CETF Jp vent			
dc-016	CETF Jp vent			
dc-017	CETF Jp vent			
dc-018	EETF Zavarzin			
dc-019	EETF Zavarzin			
dc-019a	EETF Zavarzin			
dc-020	EETF Zavarzin			
dc-021	EETF Tripool			
dc-022	EETF Tripool			
dc-023	EETF Tripool			
dc-024	CETF Shovel			
dc-025	CETF Shovel			
dc-026	CETF Shovel		1.3 or 1.4	
dc-027	CETF Shovel			
dc-028	CETF Shovel			
dc-029	CETF 13 m SE K4	0.2		
dc-030	2m SW of shovel			
dc-031	2m SW of shovel	-0.1		
dc-068	EETF Cleft Bulk			
dc-8lake	8lake mudpot			

Appendix C, Table 3
Continued

Silt Sized Fraction

Sample no.	Sample Name	Mineral δ34S (‰)				
		Pyrite	Jarosite	Sulfur	Realgar	Notes
dc-010	WTF sed/crust	xxx	x			Unable to separate
dc-015	CETF Jp vent			0.93		
dc-016	CETF Jp vent	-0.56				
dc-017	CETF Jp vent	-1.94				
dc-018	EETF Zavarzin	Trace		5.7		Not enough pyrite to analyze
dc-019	EETF Zavarzin	-0.6 and -0.6		-0.4		
dc-019a	EETF Zavarzin	1.1				
dc-020	EETF Zavarzin	0.7				
dc-021	EETF Tripool			1.9		
dc-022	EETF Tripool	Trace		0.9		Not enough pyrite to analyze
dc-023	EETF Tripool	Trace		0.9		Not enough pyrite to analyze
dc-024	CETF Shovel	3.24				
dc-025	CETF Shovel					Missing
dc-026	CETF Shovel				2.4	
dc-027	CETF Shovel				1.3	
dc-028	CETF Shovel	xxx			x	Unable to separate
dc-029	CETF 13 m SE K4	0.6 and 1.5				
dc-030	2m SW of shovel					Missing
dc-031	2m SW of shovel					Missing
dc-068	EETF Cleft Bulk	0.0		xxx		S sublimated
dc-8lake	8lake mudpot					
ps04-024	OTF	xx		xxx		Not Run
ps04-026	OTF	xxx				Not Run
ps04-029	OTF	xxx				Not Run

Appendix C, Table 3
Continued

Clay Sized Fraction

Sample no.	Sample Name	Mineral δ34S (‰) Pyrite	Sulfur	Notes
dc-010	WTF sed/crust	0.9		
dc-015	CETF Jp vent			
dc-016	CETF Jp vent			
dc-017	CETF Jp vent			
dc-018	EETF Zavarzin		0.2	
dc-019	EETF Zavarzin		xxx	No sample left
dc-019a	EETF Zavarzin	1.8		
dc-020	EETF Zavarzin	xx		
dc-021	EETF Tripool	3.8	xxx	S sublimated
dc-022	EETF Tripool	3.4	xx	S sublimated
dc-023	EETF Tripool	1.3	Minor	S sublimated
dc-024	CETF Shovel			
dc-025	CETF Shovel			
dc-026	CETF Shovel			Missing
dc-027	CETF Shovel	x	x	No sample left
dc-028	CETF Shovel			
dc-029	CETF 13 m SE K4	4.6	x	S sublimated
dc-030	2m SW of shovel			Missing
dc-031	2m SW of shovel			Missing
dc-068	EETF Cleft Bulk	3.5	xx	S sublimated
dc-8lake	8lake mudpot			
ps04-024	OTF			
ps04-026	OTF	minor		Not Run
ps04-029	OTF	0.5		

Appendix C, Table 3
Continued

Sinter and Sediment Samples

Sample no.	Sample Name	Mineral δ34S (‰)					
		Pyrite	Jarosite	Sulfur	Gypsum	Rhomboclase	Notes
JK03-010	Near outflow Channel			1.3			
Cr-Sinter	Bright white (CETF)				x	x	Unable to separate
Cr-SXV1	Vent 1 Crystals			1.1 and 1.0			
Cr-SmV2	Vent 1 JKpools			-1.3			
cr-022	Cleft EETF	x	xx				Unable to separate
cr-009	Bannoe Pool (EETF)	xx		xxx			Not Run
cr-016	bright white CETF					xxx	Not Run
cr-029	Yellowsputter EETF			1.8			
cr-041	hotblack pool	x					Not Run